

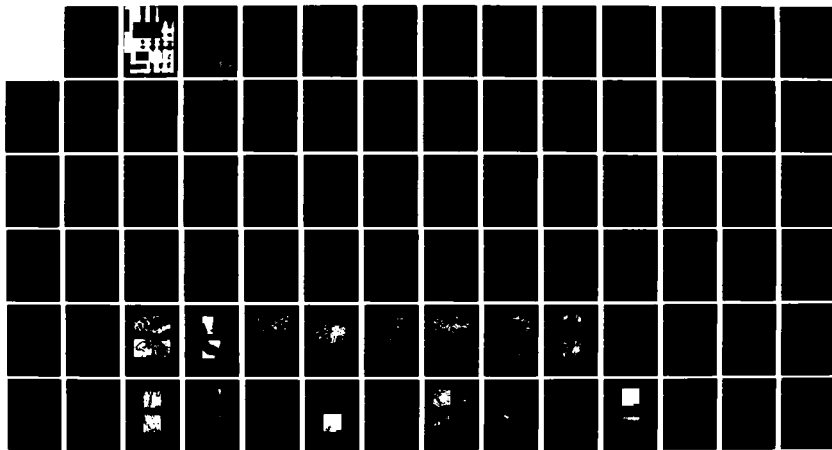
AD-A122 167

DEVELOPMENT OF HIGH MODULUS CORROSION RESISTANT
ALUMINUM ALLOYS(U) DREXEL UNIV PHILADELPHIA PA DEPT OF
MATERIALS ENGINEERING M J KOCZAK MAR 82 NADC-80100-60
N62269-80-C-0295 F/G 11/6

1/1

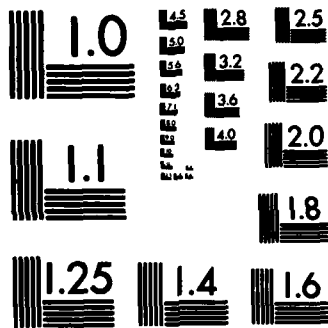
UNCLASSIFIED

NL



END

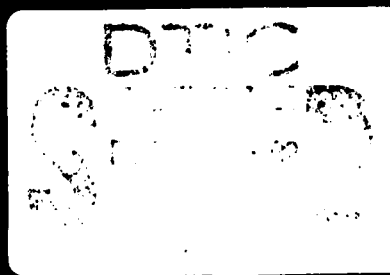
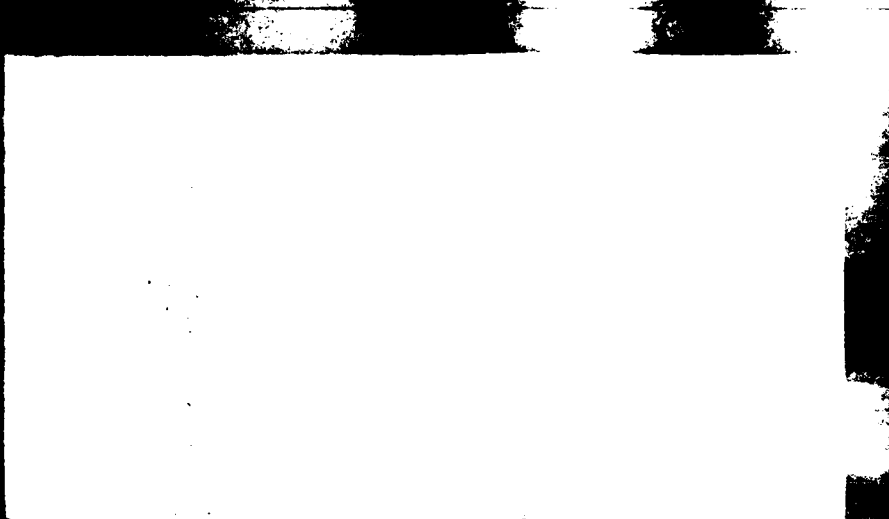
FILED
"
DTIC



MICROCOPY RESOLUTION TEST CHART
NATIONAL BUREAU OF STANDARDS-1963-A

12

AD A 122 107



DTIC FILE COPY

DISTRIBUTION STATEMENT
Approved for Distribution

NADC 80100-60

DEVELOPMENT OF HIGH MODULUS
CORROSION RESISTANT ALUMINUM ALLOYS

NADC Report #80100-60

Michael J. Koczak
Department of Materials Engineering
Drexel University
Philadelphia, Pennsylvania 19104

March 15, 1982

FINAL REPORT
(CONTRACT #N62269-80-C-0295)

APPROVED FOR PUBLIC RELEASE; DISTRIBUTION UNLIMITED

Prepared for
United States Navy
NAVAL AIR DEVELOPMENT CENTER
Warminster, Pennsylvania 18974

DTIC
ELECTE
DEC 8 1982
S B

UNCLASSIFIED

SECURITY CLASSIFICATION OF THIS PAGE (When Data Entered)

REPORT DOCUMENTATION PAGE		READ INSTRUCTIONS BEFORE COMPLETING FORM
1. REPORT NUMBER NADC 80100-60	2. GOVT ACCESSION NO. AD-A122-167	3. RECIPIENT'S CATALOG NUMBER
4. TITLE (and Subtitle) DEVELOPMENT OF HIGH MODULUS CORROSION RESISTANT ALUMINUM ALLOYS		5. TYPE OF REPORT & PERIOD COVERED Final Report for the period 8/31/80 through 7/30/81
		6. PERFORMING ORG. REPORT NUMBER
7. AUTHOR(s) Michael J. Koczak		8. CONTRACT OR GRANT NUMBER(s) N62269-80-C-0295
9. PERFORMING ORGANIZATION NAME AND ADDRESS Department of Materials Engineering Drexel University Philadelphia, Pennsylvania 19104		10. PROGRAM ELEMENT, PROJECT, TASK AREA & WORK UNIT NUMBERS
11. CONTROLLING OFFICE NAME AND ADDRESS NAVAL AIR DEVELOPMENT CENTER WARMINSTER, PA 18974		12. REPORT DATE March, 1982
		13. NUMBER OF PAGES 78
14. MONITORING AGENCY NAME & ADDRESS (if different from Controlling Office)		15. SECURITY CLASS. (of this report) UNCLASSIFIED
		15a. DECLASSIFICATION/DOWNGRADING SCHEDULE
16. DISTRIBUTION STATEMENT (of this Report) APPROVED FOR PUBLIC RELEASE; DISTRIBUTION UNLIMITED		
17. DISTRIBUTION STATEMENT (of the abstract entered in Block 20, if different from Report)		
18. SUPPLEMENTARY NOTES		
19. KEY WORDS (Continue on reverse side if necessary and identify by block number) High modulus aluminum, duplex alloy, powder metallurgy, manganese addition, 7075, X7091, extrusion, corrosion testing, mechanical testing.		
20. ABSTRACT (Continue on reverse side if necessary and identify by block number) A program of basic research has been undertaken with the overall goal of establishing quantitative processing-microstructure-mechanical behavior relationships in fully-dense duplex Al-Zn-Mg/Al-Mn alloys produced by powder metallurgy. Initial attention has been directed to powder processing, consolidation, mechanical property and corrosion response. Microstructures have been characterized in the powder, hot compacted billets, forgings and extrusions. Mechanical properties of primary interest were modulus, strength,		

DD FORM 1473
1 JAN 73EDITION OF 1 NOV 68 IS OBSOLETE
S/N 0102-LF-014-6601

UNCLASSIFIED

SECURITY CLASSIFICATION OF THIS PAGE (When Data Entered)

Impact and ductility. The goal of this highly exploratory program was to develop a duplex, aluminum alloy in which an $MnAl_6$ aluminide dispersant phase provided for modulus/strength contributions, while the Al-Zn-Mg matrix imparted ductility and toughness. The initial experimental goals were a demonstration of high modulus (80-90 GPa, 11.5-13 msi), together with ductility (5%) and strength (500 MPa, 72 ksi). Modulus and strength levels were met, and gains in ductility should be realized by finer powder size and increased levels of deformation.

A

FOREWORD

This final report summarizes the work performed by Drexel University in determining the feasibility of producing a high modulus corrosion resistant aluminum alloy. The contract, N62269-80-C-0295, is administered under the direction of Dr. Gilbert London, of the Naval Air Development Center, Warminster, PA 18974.

This report was released by the author in March, 1982 and covers the work accomplished during the period of August, 1980 through July, 1981.

Accession For	
NTIS GRA&I	<input checked="" type="checkbox"/>
DTIC TAB	<input type="checkbox"/>
Unannounced	<input type="checkbox"/>
Justification	
By	
Distribution/	
Availability Codes	
Dist	Avail and/or Special
A	

DTIC
COPY
INSPECTED
2

TABLE OF CONTENTS

	<u>Page No.</u>
LIST OF TABLES.	v
LIST OF FIGURES	vi
ABSTRACT.	1
1.0 INTRODUCTION.	2
2.0 EXPERIMENTAL PROCEDURE.	4
2.1 Material Preparation	4
2.1.1 Powder Consolidation.	4
2.1.2 Vacuum Hot Pressing (VHP)	4
2.1.3 Upset Hot Forging	4
2.1.4 Extrusion	5
2.1.5 Heat Treatment.	5
2.1.5.1 7075 T-6	5
2.1.5.2 X7091 T-6.	6
2.1.5.3 0 Temper	6
2.1.5.4 Aluminide Coarsening and T-6 for 7075.	6
2.2 Mechanical Testing	7
2.2.1 Tensile Testing	7
2.2.2 Impact Testing.	7
2.2.3 High Temperature Modulus Determinations	8
2.2.4 Metallography and Fractography.	8
2.3 Corrosion Evaluation	8
2.3.1 Open Circuit Potential Testing.	9
2.3.2 Controlled Potential Testing.	10
2.3.3 Galvanic Couple Testing	10
2.3.4 Micrographic Corrosion Assessment	11
3.0 RESULTS	12
3.1 Structure of Powders	12
3.1.1 Morphology and Topography	12

	<u>Page No.</u>
3.1.2 Microstructure.	12
3.2 Structure of Compacts, Forgings and Extrusions	13
3.2.1 Vacuum Hot Pressed Compacts	13
3.2.2 Forgings.	13
3.2.3 Billet Preform Extrusions	14
3.2.4 Direct Powder Extrusions.	14
3.3 Mechanical Properties.	15
3.3.1 Tensile Testing	15
3.3.2 Impact Testing.	17
3.3.3 High Temperature Modulus Testing.	17
3.3.4 Fractography.	17
3.4 Corrosion Evaluation	18
3.4.1 Open Circuit Potential Testing.	18
3.4.2 Controlled Potential Testing.	19
3.4.3 Galvanic Couple Testing	21
4.0 DISCUSSION OF RESULTS	22
4.1 Mechanical Property/Processing Evaluation.	22
4.1.1 Powder Characteristics.	22
4.1.2 Powder Consolidation.	23
4.2 Mechanical Property Effects.	24
4.2.1 Mechanical Characteristics of the Al-Mn Component . . .	24
4.2.1.1 Effect of Aluminide Size on Al-Mn Component. .	25
4.2.1.2 Effect of Processing on Al-Mn Component. . . .	26
4.2.1.3 Effect of Processing and Aluminide Size on Al-Mn Component.	26
4.2.2 Effect on Mechanical Properties of Powder Blend Ratio .	26
4.2.3 Mechanical Characteristics of the Duplex Alloy Matrix .	28
4.3 Modeling of Mechanical Response.	29
4.3.1 Thermal-Mechanical Processing Response.	30
4.3.2 Tensile Response.	31
4.4 Corrosion Response	32
4.4.1 Open Circuit Potential versus Time.	32
4.4.2 Controlled Potential Response	32
4.4.3 Galvanic Couple Response.	34

	<u>Page</u> <u>No.</u>
5.0 CONCLUSIONS AND FUTURE EFFORTS.	36
REFERENCES.	39
DISTRIBUTION LIST	68

LIST OF TABLES

<u>Table No.</u>		<u>Page No.</u>
I	Chemical Compositions for Alloys.	40
II	Extrusion Parameters.	41
III	Tensile Test Data for Duplex Alloys in the T-6 Condition. .	42
IV	Tensile Test Data for Duplex Alloys in the O Temper and T-6 Condition	43
V	Short Term Open Circuit Potential Test Data	43
VI	Summary of Processing Parameter/Property Relations.	44

<u>Figure No.</u>		<u>Page No.</u>
8	Impact strength, reduction in cross-sectional area, and ultimate tensile strength versus the volume percent of Al-17 ^{w/o} Mn.	53
9	Stress-strain response of direct powder extruded, 390°C (735°F), 7075 and 7075 + 20 ^{v/o} (Al-17 ^{w/o} Mn) 20:1 reduction in cross-sectional area	54
10	Stress-strain response of direct powder extruded, 390°C (735°F) X7091 and X7091 + 20 ^{v/o} (Al-17 ^{w/o} Mn), 20:1 reduction in cross-sectional area	55
11	Stress-strain response of direct powder extruded, 390°C (735°F), 0 temper, 7075 and 7075 + 20 ^{v/o} (Al-17 ^{w/o} Mn), 20:1 reduction in cross-sectional area	56
12	Stress-strain response of direct powder extruded, 390°C (735°F), 0 temper X7091 and X7091 + 20 ^{v/o} (Al-17 ^{w/o} Mn)	57
13	Normalized Young's modulus versus temperature for 7075 with varying amounts of the Al-17 ^{w/o} Mn addition	58
14	Impact fracture surface of hot upset forged 480°C (896°F) to a reduction in height of 7:1. a) 7075 + 40 ^{v/o} (Al-17 ^{w/o} Mn) b) Same as (a), but at a higher magnification	59
15	Evidence of plastic-strain incompatibility between the matrix and the Al-17 ^{w/o} Mn addition a) 0 temper 7075 b) 0 temper X7091	60
16	Electrode potential (with a saturated calomel reference) versus time for 7075, 7075 + 10 ^{v/o} (Al-17 ^{w/o} Mn), 7075 + 20 ^{v/o} (Al-17 ^{w/o} Mn) and 7075 + 40 ^{v/o} (Al-17 ^{w/o} Mn)	61
17	Microstructural results from the electrode potential test a) 7075 + 20 ^{v/o} (Al-17 ^{w/o} Mn) prior to testing b) 7075 + 20 ^{v/o} (Al-17 ^{w/o} Mn) after electrode potential testing (unetched condition)	62
18	Anodic polarization curve for the X7091 alloy and the Al-7.5 ^{a/o} Mn alloy.	63

<u>Figure No.</u>		<u>Page No.</u>
19	Microstructural results of the X7091 and the Al-7.5 a/o alloy Mn from the three electrode, potentiostatic, controlled-potential corrosion test.	64
	Potential:	
	a) E = -900 mV, X7091	
	b) E = -900 mV, Al-7.5 a/o Mn	
	c) E = -610 mV, X7091	
	d) E = -700 mV, Al-7.5 a/o Mn	
19	Microstructural results of the X7091 and the Al-7.5 a/o alloy Mn from the three electrode, potentiostatic, controlled-potential corrosion test.	65
	Potential:	
	e) E = -500 mV, X7091	
	f) E = -500 mV, Al-7.5 a/o Mn	
20	Polarization current versus time for galvanic couple of X7091 immersed in 3.5% NaCl solution opposite sample of Al-7.5 a/o Mn.	66
21	Microstructural corrosion couple results. The surface area ratio was 4:1	67
	a) X7091	
	b) Al-7.5 a/o Mn (unetched condition)	

ABSTRACT

A program of basic research has been undertaken with the overall goal of establishing quantitative processing-microstructure-mechanical behavior relationships in fully-dense duplex Al-Zn-Mg/Al-Mn alloys produced by powder metallurgy. Initial attention has been directed to powder processing, consolidation, mechanical property and corrosion response. Microstructures have been characterized in the powder, hot compacted billets, forgings and extrusions. Mechanical properties of primary interest were modulus, strength, impact and ductility. The goal of this highly exploratory program was to develop a duplex, aluminum alloy in which an $MnAl_6$ aluminide dispersant phase provided for modulus/strength contributions, while the Al-Zn-Mg matrix imparted ductility and toughness. The initial experimental goals were a demonstration of high modulus (80-90 GPa, 11.5-13 ksi), together with ductility (5%) and strength (500 MPa, 72 ksi). Modulus and strength levels were met, and gains in ductility should be realized by finer powder size and increased levels of deformation.

1.0 INTRODUCTION

Powder processed, fully dense alloys are viable and often preferred alternates to conventional cast and wrought alloys. The development of powder processed aluminum alloys has progressed on several frontiers to include (i) conventionally atomized powders producing alloys comparable to ingot metallurgy systems⁽¹⁾, (ii) the development of rapidly solidified powders for aerospace structural applications⁽²⁾, e.g. Al-Li, Al-Cu-Li⁽³⁾ and (iii) the development of aluminum alloy systems which result in a large volume fraction of an aluminide, e.g. FeNiAl₉, a particulate phase, e.g. SiC, or precipitate phase with concurrent increases in modulus and potential improvements in elevated temperature performance⁽⁴⁾. These advances have evolved from traditional ingot metallurgy systems and have not taken full advantage of the scope in alloying and processing flexibility of the powder metallurgy approach.

Traditionally, property improvement in high-performance aluminum P/M alloys has been achieved by developments in the processing technology of powder manufacture and consolidation. Alloys are usually prepared by air/inert gas atomization in which powder size, shape, chemistry and purity are more readily controlled than in chemical or electrolytic methods of production. Primary consolidation techniques for these structural powder alloys include direct compaction, e.g. hot isostatic pressing (HIP); the working of a powder preform, e.g. powder forging, extrusion; or a combination of the above. Direct powder or billet extrusions and preform forging are the currently preferred approaches for processing

aluminum powder alloys.

Advantages in aluminum P/M processing include a high materials utilization factor, fine scale microstructures, chemical homogeneity, alloying flexibility coupled with the ability to fabricate composite/duplex alloys. In the more highly alloyed compositions, it is frequently impossible to process the material by conventional ingot metallurgy approaches involving casting and working operations, consequently, alloy modifications can be produced which previously were not viable.

Recent advances in atomization have resulted in the development of Rapid Solidification Technology (RST). RST is a generic term that refers to fine, e.g. $< 40\mu\text{m}$, particulate production such that high cooling rates are achieved, typically $> 10^4\text{K/s}$. Such cooling rates result in reduced microsegregation, elimination of low incipient melt temperatures and ultra-fine microstructures. These advantages are balanced by the increased processing difficulties associated with fine powders, namely, low apparent densities, higher oxygen levels, pyrophoricity, blending and flow difficulties. The implications of RST processing are currently being examined in several alloy development programs including aluminum alloys, superalloys and specialty steels⁽⁵⁻⁷⁾.

The goals of this program were to formulate a high modulus, high strength, corrosion resistant duplex alloy system. The modulus improvement was achieved by a manganese aluminide (MnAl_6) dispersant phase, while the Al-Zn-Mg matrix (7075 or X7091) imparted the required strength, ductility and toughness. The immediate experimental goals were a combination of high modulus, e.g. 80-90 GPa, 11.5-13 ksi and matrix strength, e.g. 500 MPa, 72 ksi, coupled with adequate ductility and corrosion resistance.

2.0 EXPERIMENTAL PROCEDURE

2.1 Material Preparation2.1.1 Powder Consolidation

The aluminum powders (Table I) prepared by Gould, Cleveland, Ohio, were densified by three thermal-mechanical powder consolidation techniques: vacuum hot pressing followed by forging, vacuum hot pressing followed by extrusion and direct powder extrusion. The extrusion operations were performed by Nuclear Metals, Concord, Massachusetts. All of the resulting material was heat treated to full strength (T-6) or to an annealed (O) temper after extrusion or forging. The following subsections describe these processing operations in more detail.

2.1.2 Vacuum Hot Pressing (VHP)

The blended powder was placed in a graphite die and induction heated under vacuum (.15 Torr) to 538°C (1000°F) over a two-hour period. After a 1/2 hour hold at 538°C (1000°F), a compressive stress of 11.7 MPa (1.7 ksi) was applied to the billet and held for a 1/2 hour at constant temperature. The pressed billet was allowed to furnace cool to room temperature under vacuum. The dimensions of the vacuum hot pressed billet were approximately 100 mm (3.94 inches) high with a diameter of 120 mm (4.72 inches).

2.1.3 Upset Hot Forging

Upset forging consisted of heating a sample of VHP material in a conventional box furnace to 480°C (896°F) followed by compressive

upsetting utilizing a 150-ton Dake hydraulic press to the predetermined strains of 2:1 or 7:1. A special fixture to minimize heat loss and transfer time was constructed around the samples of VHP material. It consisted of sandwiching the VHP material between two pieces of 6.4 mm (1/4 inch) thick plate steel approximately 102 x 102 mm (4 x 4 inches square). The fixture was encased completely with Sentry stainless steel heat treating foil, wire wrapped for support and easy transport from furnace to press. The transfer time from the furnace to the press was always less than 10 seconds.

2.1.4 Extrusion

The extrusion parameters for the direct powder and VHP billet material are shown in Table II. For direct powder extrusion, the blended powder was placed in a 6061 aluminum alloy can, evacuated to less than 5×10^{-4} Torr, and heated to 330°C (625°F). The temperature was increased to 390°C (735°F) and held for 1.75 hours prior to extrusion under approximately 1.7 MN (190 ton) driving force. For VHP billet extrusions, the material was heated to 400°C (752°F) and extruded under an applied force of approximately 1.7 MN (190 ton). All extrusion samples initially had a diameter of approximately 50 mm (2 inches) and sustained a reduction in cross-sectional area of 20:1.

2.1.5 Heat Treatment

After the consolidation operations, the materials were heat treated to either the full strength (T-6) or full anneal (O temper) condition.

2.1.5.1 7075 T-6

The duplex alloy samples containing the 7075 as a matrix

constituent were heat treated to full strength as follows:

- i) Solution treatment at 465°C (870°F) for 45 minutes,
- ii) rapidly quenching in water at 25°C (78°F),
- iii) aging at 25°C (78°F) for 24 hours, and
- iv) aging at 120°C (250°F) for 24 hours.

2.1.5.2 X7091 T-6

For the duplex alloy samples containing the X7091 as a matrix constituent, the heat treatment to full strength was as follows:

- i) Solutionize at 488°C (910°F) for 45 minutes,
- ii) rapidly quench in ice water,
- iii) allow samples to age at 25°C (78°F) for 5 days,
- iv) aging at 120°C (250°F) for 24 hours, and
- v) aging at 163°C (325°F) for 4 hours.

2.1.5.3 0 Temper

The samples that were to be fully annealed were:

- i) Heated to 413°C (775°F) for 3 hours, and
- ii) cooled in air.

2.1.5.4 Aluminide Coarsening and T-6 for 7075

To ascertain if the size of individual aluminides in the Al-17 w/o Mn powder had an effect on the mechanical properties of the duplex alloy, an extended solutionizing treatment was used on one set of samples to coarsen the intermetallics:

- i) Solutionize at 465°C (870°F) for 6 hours,
- ii) rapidly quench in water,
- iii) age at room temperature for 24 hours, and
- iv) age at 120°C (250°F) for 24 hours.

After the material was heat treated, the samples were prepared for mechanical testing.

2.2 Mechanical Testing

The mechanical properties of the alloys produced (see Section 2.1) were evaluated by tensile, impact and high temperature flexural modulus testing. The failed specimens were examined using optical and electron microscopy. The following subsections describe in greater detail the testing and observation procedures.

2.2.1 Tensile Testing

Two types of tensile specimen were used: Tensile bars from the forgings were of 6.35 mm (0.25 inch) gage length, a 6.35 mm (0.25 inch) diameter, and a 127 mm (5 inches) radius of fillet; while extrusion tensile bars had a 25.4 mm (1 inch) gage length, a 6.3 - 7.6 mm (0.25 - 0.3 inch) diameter, and a 4.8 mm (0.2 inch) radius of fillet.

The specimens were tested using an Instron tensile testing machine at room temperature, using an Instron extensometer system calibrated to provide a 500:1 magnification on the strain axis. The specimens were loaded at a crosshead speed of 0.5 mm (0.02 inch) per minute.

2.2.2 Impact Testing

Impact tests were performed using a standard Charpy machine operating on its high scale (240 ft.lbs. full scale). Standard size (ASTM 23) Charpy, V-notched test specimens were machined from the forgings. Impact specimens were not machined from the extrusions because the diameter of the extrusions was insufficient for a standard size specimen.

2.2.3 High Temperature Modulus Determinations

A Dupont 1090 Differential Mechanical Analysis apparatus was used to measure the elastic modulus between room temperature and 450°C. The change of modulus with temperature was recorded for 7075 and three 7075 based alloys, containing 10, 20 and 40 v/o of Al-17 w/o Mn.

2.2.4 Metallography and Fractography

Optical metallography was performed on samples of each material before and after tensile testing. Samples were mounted using a fine glass-filled bakelite powder. The specimens were polished using standard metallographic techniques and then etched with either of the following:

i) Keller's Reagent

1.0 ml HF (conc)

1.5 ml HCl (conc)

2.5 ml HNO₃ (conc)

95 ml H₂O

ii) Graff-Sargent's Reagent

0.5 ml HF (conc)

15.5 ml HNO₃ (conc)

84 ml H₂O

3.0 g CrO₃

2.3 Corrosion Evaluation

The experimental program for corrosion evaluation consisted of examining the electrochemical behavior of a high strength Al-Zn-Mg alloy, X7091, and a high modulus Al-Mn alloy. In addition, an experimental duplex alloy of 7075 with a 20% addition of Al-17 w/o Mn was studied. The corrosion environment for these examinations was a 3.5%

solution of NaCl in distilled, de-ionized water open to the laboratory atmosphere at room temperature. The samples for evaluation of electrochemical behavior were cold mounted in a quick setting epoxy resin, and the exposed surface of each test sample was polished using standard metallographic techniques. This eliminated any differences due to surface quality and permitted the metallographic examination of the samples following corrosion evaluation, revealing the microstructure, the mode, and mechanism associated with corrosion.

The techniques for evaluating the electrochemical behavior of the samples were an open circuit potential versus time test, a controlled potential corrosion test, and a galvanic couple test. Each of these techniques is discussed in the following subsections.

2.3.1 Open Circuit Potential Testing

The open circuit potential versus time test incorporates a working electrode and a reference electrode. The working electrodes were the test samples mounted on a conventional electrode holder through a teflon gasket. The samples had one face 12.7 x 12.7 mm (0.5 x 0.5 inch) exposed. A saturated calomel electrode (S.C.E.) was used as a reference electrode. These electrodes were connected together via a high resistance voltmeter known as an "electrometer". Such a meter was used so that potentials can be measured between the electrodes with virtually no current flow (open circuit). This electrode potential data was recorded as a function of time. The test started upon immersion of the working and reference electrodes in the 3.5% NaCl solution.

These measured values are valuable when examining the microstructural characteristics that each alloy exhibited while corroding.

Also, this data was used in determining the set potentials for the controlled potential experiments.

2.3.2 Controlled Potential Testing

The controlled-potential corrosion technique⁽⁸⁾ employs a working electrode, a counter electrode and a reference electrode. The working electrodes were the test samples similar to those used for the open circuit tests, mounted on a conventional electrode holder through a teflon gasket. A saturated calomel electrode (S.C.E.) was used as the reference, and a platinum electrode was used as the counter. The test sample was maintained at a predetermined constant set potential with respect to the S.C.E. reference. Constant set potentials and corresponding polarizing currents were maintained potentiostatically using the platinum counter electrode. The polarizing current was recorded as a function of time upon immersion of the electrodes into the 3.5% NaCl solution.

From this experiment it was possible to determine the sites of preferential attack in the microstructure at each set potential. These potentials were chosen to be in the vicinity of the open circuit potentials determined in the previous experiment (Section 2.3.1).

2.3.3 Galvanic Couple Testing

The galvanic couple test uses two working electrodes, each having only one face exposed. The couple consisted of a sample of X7091 and a sample of Al-7.5 % Mn with an exposed area ratio of 4:1. The working electrodes were constructed by attaching the test samples to a standard electrode holder through a teflon gasket. This test consisted of measuring the current flowing between the two electrodes upon immersion into the 3.5% NaCl solution using a zero-resistance ammeter. The

zero-resistance ammeter was constructed by potentiostatically maintaining a zero potential between the samples and recording the current output as a function of time.

2.3.4 Micrographic Corrosion Assessment

The test samples from all of the corrosion tests were examined using optical microscopy to determine the regions of preferential attack. Samples tested at various potentials were ultrasonically cleaned in distilled water, forced air dried and microscopically examined after the open circuit potential test, the controlled-potential test, and the galvanic couple test.

3.0 RESULTS

3.1 Structure of Powders

3.1.1 Morphology and Topography

Samples of the atomized metal powders were examined using a scanning electron microscope with EDAX facility. This instrument is well-suited to surface examinations as it combines an analytical capability with high resolution and good depth of field. Typical observations are shown in Figure 1(a) to 1(d). The general morphology of both the 7075 and the Al-17 W/o Mn powders at 100x magnification is shown in Figure 1(a) and 1(c). It may be seen that although the powders are irregularly shaped, the particles are generally rounded. This is consistent with air atomized aluminum powder.

Examination of the powder surfaces at higher magnification (300x) reveals a considerable difference between the powders. This difference may be seen by comparison of Figure 1(b), which shows the relatively smooth surface of the 7075 powder, with Figure 1(d) which shows the rough, virtually acicular, surface of the Al-17 W/o Mn powder. The roughness of the Al-17 W/o Mn alloyed powder surface is attributed to the $MnAl_6$ intermetallics protruding from the surface.

3.1.2 Microstructure

Samples of the powders were mounted, polished and etched in preparation for metallography. The X7091 and 7075 powders were generally consistent, displaying a fine, cast, cellular structure; an ex-

ample of 7075 is shown in Figure 2(b). The microstructure of the Al-17 w/o Mn powder consisted of an FCC Al matrix with a dispersed $MnAl_6$ intermetallic phase. The size of the intermetallic was found to be extremely sensitive to powder size, the $MnAl_6$ becoming finer as the powder particle size decreased. An example of the $MnAl_6$ microconstituent size variation is shown in Figure 2(a), which compares a coarse and a fine powder particle.

3.2 Structure of Compacts, Forgings and Extrusions

3.2.1 Vacuum Hot Pressed Compacts

Samples of the vacuum hot pressed preforms containing various proportions of 7075 and the Al-17 w/o Mn powders were examined using optical microscopy. The microstructures observed are shown in Figure 3 where it can be seen that powder particle boundaries are delineated by oxide films and that the structures contain residual porosity. These vacuum hot pressed compacts served as preforms for subsequent forging/extrusion operations

3.2.2 Forgings

The effect of hot upset forging on three of the preform compositions (10, 20 and 40 v/o Al-17 w/o Mn) at two forging height reductions (2:1 and 7:1) was studied. The effect of the 2:1 reduction on the microstructures is shown in Figure 4, while the result of the 7:1 reduction is presented in Figure 5.

Comparison of the microstructures reveals that the aspect ratio change induced in the Al-17 w/o Mn powder particles is not solely dependent on the reduction ratio; the fineness of the aluminide phase appears to have a significant effect. The smaller Al-17 w/o Mn powder

particles, which contain the finer aluminides, show considerably more elongation on forging compared to the larger powder particles with the coarser aluminides (see Section 3.1.2). This phenomenon is well demonstrated by Figure 5(c), which shows that even after a 7:1 forging reduction, the larger Al-17 w/o Mn powder particles remained relatively undeformed, while the immediately adjacent smaller particles show considerable flow.

It should also be noted that the strain imparted in both the forging treatments was sufficient to break up the continuous oxide films and to produce fully dense microstructures.

3.2.3 Billet Preform Extrusions

An alternative to upset hot forging of vacuum hot pressed compacts is extrusion. Compacted billets of four powder blends were hot worked in this manner, giving an extrusion ratio of 20:1. Figure 6 shows the microstructures obtained by this technique. It may be seen that considerably more plastic deformation was introduced into the structure vis-a-vis upset hot forging. This deformation produced a fully dense structure and completely disrupted the powder particle oxide films. In the blended powders (Figure 6(b) and 6(d)), a considerable degree of elongation of the aluminide containing powder particles has occurred, resulting in a clearly oriented structure. It should be noted, however, that the elongation of the Al-17 w/o Mn powder is again (see Section 3.2.2) strongly dependent on the powder size, i.e. the fineness of the aluminides within the powder particle (see Section 3.1.2).

3.2.4 Direct Powder Extrusions

This processing technique circumvents vacuum hot pressing.

The unconsolidated powder blends were canned in a 6061 aluminum and directly extruded at 390°C using a 20:1 reduction of area ratio. These extrusion conditions were virtually identical to those for the billet extrusions (Section 3.2.3) which permitted direct comparison of the structures obtained from the two extrusion methods.

The microstructures of two of the direct extrusions are shown in Figure 7. It may be seen that both of these blended powder direct extrusions appear to be microstructurally similar to their billet extruded counterparts (Figure 6). The direct extrusions exhibit good consolidation characteristics, but again a variation in strain between various Al-17 w/o Mn powder particles is visible.

3.3 Mechanical Properties

Mechanical properties were evaluated for a variety of powder blends and processing techniques. The mechanical property data is presented in Tables III and IV and graphically summarized in Figure 8.

Table III and Figure 8 show the dependence of tensile and impact behavior on the volume fraction of Al-17 w/o Mn addition to 7075 in the T-6 condition. This data also shows the effect of processing technique and aluminide size on mechanical response.

Table IV presents tensile test data for four powder blends: 7075, X7091, 7075 + 20 v/o (Al-17 w/o Mn), X7091 + 20 v/o (Al-17 w/o Mn). This data set shows the difference in mechanical properties between the T-6 and 0 temper conditions. The following subsections more fully describe the data obtained from the various tests.

3.3.1 Tensile Testing

The Al-17 w/o Mn powder additions are principally intended

to increase the modulus of the resultant duplex alloys. Referring to Tables III and IV and Figures 8 to 12, it may be seen that this objective has been achieved, all of the duplex Al-Zn-Mg/Al-Mn alloys showing improved modulus compared to their Al-Zn-Mg counterparts. Table III indicates that for 7075 in the T-6 condition the modulus improvement increases as the volume fraction of Al-17 W/o Mn increases. The data also reveals that the modulus improvement is largely independent of the temper condition of the 7075 or X7091. This improvement in modulus, however, has been attained at the expense of some of the other properties, e.g. ductility and toughness.

Table III and Figure 8 show that for 7075 in the T-6 condition the presence of the aluminides reduces the ductility, yield and ultimate strength, these properties decreasing with increasing aluminide content. For example, it may be seen that the ultimate tensile strength initially drops rapidly with increasing Al-17 W/o Mn volume fraction, but tends to level off after approximately 20 V/o for the forged and directly extruded materials. The ductility, as represented by the reduction of area, becomes negligible after 10 V/o addition in both the coarsened and uncoarsened material.

Table IV presents the data for the 0 temper and T-6 condition. The data indicates that the 0 temper yield strength is slightly improved by the presence of the aluminides, however, the ultimate tensile strength and ductility are again reduced. It should be noted that in the 0 temper condition, the 20 V/o alloys show significant ductility, 5.3% and 6.6% elongation for 7075 and 7091 respectively.

3.3.2 Impact Testing

Referring to Figure 8, it is possible to see that the impact resistance of the duplex alloys decreases as the proportion of the Al-17 w/o Mn powder in the blend increases and that this effect becomes more pronounced with the coarser aluminides. It should be noted, however, that the alloys still retain measurable impact resistance even with high volume fractions of aluminides.

3.3.3 High Temperature Modulus Testing

The Young's Moduli for 7075 and three 7075 based duplex alloys containing various volume fractions of Al-17 w/o Mn were determined at temperatures ranging from 30° to 460°C. The results from these experiments are graphically summarized in Figure 13 where the Young's Moduli, normalized relative to that of 7075, are plotted versus temperature. It may be seen that at temperatures below 380°C the relative values of the alloy moduli agree with those measured by the conventional tensile tests (Section 3.3.1), i.e. the modulus at any temperature increases with increasing aluminide content. Also, in this temperature range, the moduli of all of the alloys decrease steadily with increasing temperature.

At temperatures in excess of 380°C the relative positions of the plots began to change, the modulus values of the duplex alloys being observed to decrease more rapidly than for 7075. This effect is of such a magnitude that above 420°C the modulus of the 10 v/o duplex alloy falls below that of 7075.

3.3.4 Fractography

Scanning electron microscopy and optical metallography were used to examine the failure mode of the impact and tensile specimens.

Typical electron micrographs of an impact specimen fracture surface are presented in Figure 14. These show the operation of a mixed fracture mechanism: a brittle, transgranular mode through the Al-17 W/o Mn areas and a ductile transgranular failure mode operating in the 7075 matrix.

Optical micrographs on longitudinal sections were taken near the fracture in tensile specimens. These revealed that the fracture originated by cracking of the Al-17 W/o Mn phase. The number and size of the cracks was found to be a function of the degree of consolidation induced elongation of the Al-17 W/o Mn phase. It was observed that elongated aluminide areas showed a number of small cracks, suggesting the operation of a good load transference mechanism between the phases. Conversely, the unelongated areas, i.e. originally large Al-17 W/o Mn powder particles, usually showed a gross, solitary fracture. This phenomenon was particularly prevalent in the 0 temper condition. An example of this is shown in Figure 15.

3.4 Corrosion Evaluation

3.4.1 Open Circuit Potential Testing

The results of short term open circuit potential testing of X7091 and Al-7.5 a/o Mn alloy are summarized in Table V, while the open circuit potential versus time tests for 2:1 forged, solutionized and aged 7075 with various volume fractions of Al-17 W/o Mn are graphically summarized in Figure 16.

In the short term tests, X7091 represented the matrix component of the X7091 based duplex alloys, while the Al-7.5 a/o Mn was equivalent to the aluminide containing powders. The results show that the X7091 has an average open circuit potential of approximately -840 mV

with respect to a saturated calomel electrode (S.C.E.) and that the Al-7.5 a/o Mn has a value of -960 mV S.C.E. These open circuit potential values indicate that the aluminide areas in the duplex alloys are anodic to the X7091 matrix.

In the Open Circuit Potential versus time tests, the plots presented in Figure 16 show that the average potential of the duplex alloys becomes more negative, or anodic, with increasing aluminide volume fraction. This is consistent with the short term Open Circuit Potential tests which showed the Al-7.5 a/o Mn to be anodic to the X7091. The long term data also shows that there is considerable variation of the potential with time, particularly in the duplex alloys.

Microscopic examination of the specimens used for Open Circuit Potential versus time tests revealed that, in all cases, the most severe attack took place at the 7075/Al-17 w/o Mn interfaces. This preferential attack was observed in the form of pitting; a typical example of this is shown in Figure 17.

3.4.2 Controlled Potential Testing

Using the potentials obtained during the Open Circuit Potential Tests (see Section 3.4.1) for reference, several potentials were selected for controlled potential testing of the X7091 and Al-7.5 a/o Mn alloy. The results of the controlled potential testing are graphically summarized in Figure 18 when it may be seen that for both alloys, raising the potential increased the corrosion rate as expressed by the current density. The data would also indicate that for any potential below -500 mV S.C.E., the manganese aluminide sample displayed a higher current density.

The samples used in this portion of the investigation were polished prior to testing, thus permitting subsequent metallographic examination. Typical micrographic observations are shown in Figure 19, which demonstrates that the nature and extent of attack during testing were strong functions of the applied potential and the alloy composition. This dependency is illustrated by comparing the surfaces of the two alloys at each testing potential.

At -900 mV S.C.E., the X7091 exhibits slight grain boundary delineation in combination with general surface attack (Figure 19(a)). Conversely, at the same potential, the Al-7.5 a/o Mn alloy shows isolated, but quite deep, pitting (Figure 19(b)).

Changing the potential to -700 mV S.C.E. slightly alters the attack on X7091. This may be seen in Figure 19(c) where there is still some grain boundary attack but far less generalized corrosion. In comparison, the Al-7.5 a/o Mn alloy begins to show significant attack at the aluminide/aluminum interfaces, resulting in the leaching out of some particles (Figure 19(d)). This trend towards pitting attack on the manganese aluminide alloy and more uniform attack on the X7091 was observed to continue on increasing the potential to -610 mV S.C.E.

At -500 mV S.C.E., the degree and nature of attack on the two alloys became drastically different, although it should be noted that the actual corrosion rates (current densities) are identical. This disparity may be seen by comparing Figure 19(e) with 19(f), the X7091 displaying virtually uniform attack with only minor pitting, while the Al-7.5 a/o Mn alloy exhibits deep pitting at sites where aluminide particles have been leached out.

3.4.3 Galvanic Couple Testing

In these tests, the polarizing current as a function of time was measured for a corrosion couple consisting of X7091 immersed in a 3.5% NaCl solution opposite a sample of Al-7.5 a/o Mn. The results obtained are graphically summarized in Figure 20, where it can be seen that the current was generally in the range of 0.25 μ A and rarely exceeded 1 μ A.

The samples were examined microscopically after testing. It was found that the surface appearance was very similar to that of the Controlled Potential specimens tested at -900 mV S.C.E. This may be seen in Figure 21 where the X7091 exhibits general corrosion with slight grain boundary delineation, while the Al-7.5 a/o Mn alloy displays irregular, heavy pitting.

4.0 DISCUSSION OF RESULTS

4.1 Mechanical Property/Processing Evaluation

The objective of this research program was to develop a high modulus aluminum coupled with strength, good ductility and corrosion resistance, produced and processed by conventional powder metallurgy techniques.

To date, the work has concentrated on alloy design and processing experiments to assess the feasibility of producing a duplex alloy containing Al-Mn additions in an Al-Zn-Mg 7075 type matrix. It has been shown that these trial alloys could be atomized, consolidated, forged and extruded by normal industrial processes. The ductility in the T-6 tempers of these initial alloys is, however, limited, and areas for ductility improvements shall be discussed.

In the following subsections, the effect of production techniques on structure-property relationships is described and the observed trends discussed. The trends are shown to be in agreement with existing theories for modeling mechanical behavior, hence providing an understanding of the mechanisms governing the mechanical response of the alloys. These considerations permit guidelines to be established for alloy structure and composition optimization.

4.1.1 Powder Characteristics

All of the powders used in these initial experiments were air atomized producing fully dense powders of irregular shape without any

reaction problems being encountered. The ability to use this production technique is an advantage, since air is the least expensive atomization medium vis-a-vis helium and produces an Al-Zn-Mg powder which may be conventionally processed.

Microstructurally, the resulting 7075 and X7091 powder particles were found to be homogeneous and uniform. Conversely, the size of the $MnAl_6$ intermetallics in the Al-17 w/o Mn powder was found to be dependent on the powder particle size, the aluminide size increasing with increasing powder size, hence decreasing cooling rate. This aluminide size variation may be attributed to the influence of powder particle size on cooling rate, therefore the $MnAl_6$ nucleation kinetics.

The Al-17 w/o Mn powder has a high modulus by virtue of the 66 v/o of the very hard $MnAl_6$ present in the powder. The objective of blending this powder with 7075 or X7091 powder was to improve the modulus of the final duplex alloy. In order to assess an optimum proportion of Al-17 w/o Mn, a range of powder blends was prepared and subsequently evaluated.

4.1.2 Powder Consolidation

The results show that three consolidation techniques can be utilized to produce an alloy with a wide range of final microstructure and properties. Some form of hot working is invariably required to disrupt the oxide films and produce full density aluminum powder products. Three deformation schedules were studied: a 2:1 forging reduction, a 7:1 forging reduction and a 20:1 extrusion of powders and consolidated billets. The object of these varying amounts of strain was to determine the effect of hot working on the oxide films and the morphology and

distribution of the Al-17 w/o Mn component. The results show (Section 3.2) that even relatively small strains cause full densification and that the duplex alloy is workable, with little evidence of cracking or void formation associated with the Al-17 w/o Mn. The results also show that the aspect ratio of the Al-17 w/o component was a function of the strain. The $MnAl_6$ phase and the surrounding Al-Mn was easily drawn out in the direction of working. This aspect ratio change was also noted to be strongly dependent on the $MnAl_6$ precipitate size, showing less elongation with increasing intermetallic size.

4.2 Mechanical Property Effects

One of the novel aspects of this program is the flexibility of the powder approach used which permits independent and relatively easy control of the duplex alloy microstructural characteristics. The following discussion will correlate the effect of each microstructural parameter with the observed mechanical response. These adduced effects will then be compared to those predicted from theoretical considerations (Section 4.3).

4.2.1 Mechanical Characteristics of the Al-Mn Component

The first factor to be considered is the intrinsic properties and nature of the Al-17 w/o Mn powder component of the duplex alloys. The rationale for this powder is that additions of manganese to aluminum increase the modulus dramatically, the effect being second only to that of lithium. In dilute alloys, the extent of this improvement is proportional to the amount of manganese in solid solution. The modulus improvement continues even when the $MnAl_6$ intermetallic forms with the elastic properties of the aluminides exerting their influence on the

resulting alloy. The effective transference of elastic properties from the $MnAl_6$ to the alpha-aluminum matrix depends on the size and shape of the aluminides and their interface coherency with the Al-Mn matrix. The Al-Mn alloy as a whole in turn transfers its elastic contribution to the matrix of the duplex alloy, this process again depending on the size, shape and interface of the Al-Mn alloy component.

The experimental fabrication method influenced both the size and shape of the individual aluminides and the Al-Mn alloy component areas. An appraisal of the system diffusion kinetics suggests that while the processing variables affect the morphology and distribution of the components, the nature of their interfaces remained constant. The results indicate that for both the aluminides and the Al-Mn component areas, a fine, oriented, high aspect ratio structure gives the optimum properties. The evidence for this conclusion was illustrated by the experiments described in Sections 4.2.1.1 and 4.2.1.2.

4.2.1.1 Effect of Aluminide Size on Al-Mn Component

The first experiment compared data from coarsened and uncoarsened duplex alloys in the T-6 condition, containing similar volume fractions of the Al-17 W/o Mn component, given similar strains during consolidation. In this comparison, the Al-Mn component areas were of similar aspect ratio, but in one case, the $MnAl_6$ aluminides had been deliberately coarsened. The results show the coarsened alloys to have distinctly inferior properties. It should be noted that the effect of aluminide size on crack propagation in the Al-Mn component was not considered a major influence in this case.

4.2.1.2 Effect of Processing on Al-Mn Component

The second set of data to be compared is for alloys containing $MnAl_6$ aluminides of similar sizes but which had experienced different strains during consolidation. This introduced varying degrees of strain induced aspect ratio change in the Al-17 w/o Mn components. The results show that the extrusions had better properties than the 7:1 forgings, which in turn had better properties than the 2:1 forgings. The improved properties are a direct result of the higher aspect ratio duplex phase coupled with an improved interparticle bonding and oxide film disruption. It should be noted that the modulus was unaffected by the morphology and distribution of the duplex alloy components, as it is predominantly dependent on the quantity of the alloying additions.

4.2.1.3 Effect of Processing and Aluminide Size on Al-Mn Component

Thus it may be concluded that for optimum properties, the Al-Mn component should be fine and elongated, which implies that a small powder size and high extrusion ratios are beneficial. The increasing cooling rate with decreasing particle size during atomization would cause a reduction in the size of $MnAl_6$, which in turn not only has better properties per se, but also leads to higher aspect ratios in the Al-17 w/o Mn powder particles during consolidation. It may therefore be seen that there is a strong motivation to atomize very fine Al-Mn powder. The size effect may further be enhanced by the use of helium atomization which gives a more rapid cooling rate than air.

4.2.2 Effect on Mechanical Properties of Powder Blend Ratio

Comparison of the results within any data group that has Al-17 w/o Mn additions of similar characteristics permits the effect of

the volume fraction of the addition to be deduced. The object in varying the quantity of the Al-17 w/o Mn addition was to ascertain what level would provide a worthwhile improvement in modulus without excessively compromising the ductility and toughness of the resulting duplex alloy. It was found that the modulus of the duplex alloy, as expected, increased with increasing additions of the Al-Mn component. This indicates good stress transference is occurring between the components of the duplex alloy.

In the Al-17 w/o component, the stress concentration imposed on the alpha-aluminum by the rigid $MnAl_6$ aluminides will result in extremely limited ductility at room temperature. Thus, it would be anticipated that if good stress transference is occurring between the components in the duplex alloy, then the strain incompatibility between the components will lead to localized stressing of the Al-Mn component areas, hence cracking at high stresses. Further increases in stress cause these cracks to propagate through the matrix resulting in a rapid, low ductility failure. This mechanism accounts for the decrease in strength and ductility observed with increasing volume fractions of the Al-17 w/o Mn.

The results indicate that the optimum balance between increased modulus and acceptable strength and ductility lies around 20 v/o. The ductility and strength of these 20 v/o alloys can be improved by modifying the structure of the Al-17 w/o Mn to increase its capacity for plastic strain at room temperature. One approach to achieving this improvement in ductility would be to decrease the aluminide size by methods similar to those outlined in Section 4.2.1.3. Alternatively, the embrittling effect of each aluminide may be decreased by increasing the deformable volume

surrounding it. At the cost of a certain amount of flexibility in production, this could be achieved by pre-alloying the 7075 or X7091 powder with Mn prior to atomization. The constitutional chemistry of such an alloy would require careful consideration so as not to significantly impair the eta-phase precipitation response.

4.2.3 Mechanical Characteristics of the Duplex Alloy Matrix

The final parameter to be varied in the experimental work was the matrix of the duplex alloys, four matrix variations being studied: 7075 (T-6), X7091 (T-6), 7075 (O temper) and X7091 (O temper). A comparison of these four matrix permutations for a series of 20 v/o duplex alloy extrusions may be found in Table IV. In general, it may be seen that there was little difference in mechanical response between the two matrix alloys in the same temper condition. Conversely, a significant difference in properties was observed between the two temper conditions.

In the T-6 (full strength) condition, both of the duplex alloys exhibited their maximum yield and ultimate strengths, which were lower than for the matrix phases alone. The duplex alloys also did not have the considerable ductility of their respective matrix phases in the T-6 condition. The low ductility observed is attributed to crack formation occurring in the Al-Mn areas by a stress transference mechanism, the cracks then growing rapidly through the matrix resulting in a low ductility failure.

In the O temper condition, the yield strength of the duplex alloys was slightly higher than that of the matrix alloys; however, the ultimate strength and ductility were again significantly lower. It should be noted that this temper condition shows that the duplex alloys

have an appreciable amount of inherent ductility. In this case, flow of the matrix phase occurs around the relatively undeformable Al-Mn areas until a stress is reached at which cracks develop in the brittle Al-Mn. These cracks would not be expected to propagate so rapidly as in the T-6 condition, since the softer matrix may provide some "crack blunting". The O temper condition revealed one of the few differences between the two matrix alloys: the 7075 (T-6) duplex alloys showing a more uniform crack distribution in the Al-17 w/o Mn areas than X7091 based alloys. This phenomenon is thought to be a feature of the stress transference occurring within the alloys but has yet to be fully explained.

The modulus of the duplex alloys was found to be relatively insensitive to the matrix alloy and its temper condition. This would be expected, as modulus is principally related to the quantity of the solute elements. The improvement in modulus observed in the duplex alloys is therefore dependent on stress transference to the aluminides by the matrix resulting in the cracking of the Al-17 w/o Mn phase observed at room temperature.

4.3 Modeling of Mechanical Response

The flow stress and strain characteristics of the experimental duplex alloy during thermal-mechanical processing and tensile testing correspond well with the existing theories for predicting the yield strength of two-phase alloys with coarse microstructure. The dependency of the yield stress of a two-phase alloy on the size and distribution of the second phase and its connectivity in the microstructure has been qualitatively modeled by Gurland.^(9, 10) The model, essentially an

empirical rule of mixtures, takes into account the load transfer between alloy constituents and their respective yield strengths and assesses the effects in terms of microstructure geometry. The mathematic representation of Gurland's approach for analyzing the yield stress of a two-phase alloy is as follows:

$$\bar{\sigma}_y = \sigma_{\alpha e} (1 - C_{\beta} f_{\beta}) + \sigma_{\beta C} C_{\beta} f_{\beta} \quad (1)$$

where $\bar{\sigma}_y$ is the apparent yield strength of the two-phase alloy, $\sigma_{\alpha e}$ is the effective strength of the continuous α phase, $\sigma_{\beta C}$ is the strength of the contiguous β phase, C_{β} is a factor relating the degree of contiguity of the β phase, and f_{β} is the volume fraction of the β phase present in the alloy. The factor, C_{β} , can equal any number from zero for a completely isolated, unconnected β phase to unity for a completely connected β phase. The term $(1 - C_{\beta} f_{\beta})$ represents the volume fraction of α and non-contiguous β phase; $C_{\beta} f_{\beta}$ represents the volume fraction of the contiguous β phase.

4.3.1 Thermal-Mechanical Processing Response

The size dependent flow characteristics of the Al-Mn powder particles during thermal-mechanical processing of the duplex alloys may be explained by Gurland's model. The differences in the flow characteristics may be attributed to the average size and contiguity of the manganese aluminides in the individual Al-17 W/o Mn particles. Gurland's model implies that in the Al-17 W/o Mn addition, where the continuous phase is α -aluminum and the dispersed hard phase is MnAl_6 , the flow stress of the particles is dependent on the amount of contiguity of the MnAl_6 phase. In the small Al-Mn powder particles where the manganese

aluminides are small and unconnected, C_g is equal to zero; the flow stress, as given by equation 1, is equal to the effective strength of the continuous α -aluminum phase. In the larger particles where the manganese aluminides are larger and connected, C_g approaches one, and thus the flow stress becomes a function of both the effective strength of the α -aluminum and the strength of the $MnAl_6$. Hence elongation of the Al-Mn component during processing is a function of the aluminide contiguity, which is observed to increase with increasing aluminide size.

4.3.2 Tensile Response

The mechanical response model developed by Gurland may be used to analyze the tensile response of two-phase alloys with coarse microstructure. The experimental results for the duplex alloys show that the tensile strength increases with increased thermal-mechanical processing, which is in accordance with Gurland's model. For example in the forged material where the Al-17 w/o Mn addition had not deformed appreciably, Gurland's model predicts a tensile strength close to that of the effective tensile strength of the 7075, since the Al-17 w/o Mn addition is discontinuous. Conversely, the extruded materials where the Al-17 w/o Mn addition had deformed appreciably should have a tensile strength that is a function of the strength of the matrix and the addition, since the Al-17 w/o Mn addition is now more contiguous in the direction of loading. The higher contiguity of the Al-17 w/o Mn addition in the direction of loading results in better load transfer between the matrix and Al-Mn addition.

4.4 Corrosion Response

4.4.1 Open Circuit Potential versus Time

The results from the open circuit potential test for X7091 and Al-7.5 a/o Mn showed that the Al-Mn is anodic with respect to the X7091.

The results of the open circuit potential versus time test on the 7075 and 7075 with 10, 20, and 40% Al-17 w/o Mn addition were presented in Figure 16. The curves show that the average potential of the duplex alloy becomes more negative or anodic with increasing addition of Al-17 w/o Mn. The randomness of the curves for the duplex alloys may be attributed to the inhomogeneity inherent in these alloys. Figure 17 shows typical microstructures of a 7075/Al-17 w/o Mn duplex alloy in the as-received condition and after the electrode potential versus time test. The photomicrographs show that the 7075 has been cathodically polarized by the Al-Mn alloy segments, resulting in the 7075/Al-17 w/o Mn interface pitting while the interior of the Al-Mn addition is almost pit-free.

4.4.2 Controlled Potential Response

The open circuit potential test showed a variation with time; as a consequence, the attack of any particular phase or microstructural feature cannot be directly related with any one potential. However, every individual phase of an alloy has its own characteristic polarization behavior, and a potential exists at which one particular phase corrodes preferentially. With the controlled potential approach, the characteristic corrosion behavior of any alloy can be determined, thereby identifying the microconstituent that corrodes preferentially.

The controlled potentials used for evaluation ranged from -900 mV to -500 mV. These potentials were chosen for their proximity to the average open circuit potentials determined for X7091 and Al-7.5 a/o Mn. At a controlled potential of -900 mV S.C.E., the X7091 is cathodically polarized. The reaction at the surface of the cathode is the formation of hydrogen gas which strips the thin protective aluminum oxide film from the surface of the X7091 and accounts for the uniform attack of the specimen surface in Figure 19(a). Also, signs of preferential attack are evident in the grain boundaries of X7091 at the precipitates within the grains and in the groups of precipitates associated with the grain boundaries.

At a controlled potential of -900 mV S.C.E., the Al-7.5 a/o Mn is anodically polarized. The reaction at the surface of the anode is the dissolution of the metal. The thin protective aluminum oxide film on the surface of the Al-7.5 a/o Mn sample has not been totally breached as it was on the X7091 sample. In these areas, the manganese aluminide- α aluminum interface or possibly the manganese aluminide itself may be preferentially attacked (Figure 19(b)).

At -700 mV S.C.E., the Al-7.5 a/o Mn alloy exhibits reduction of select areas of the thin aluminum oxide film and preferential attack associated with the manganese aluminide particles. This attack may be at the interface of the manganese aluminide- α aluminum matrix (Figure 19(d)), and/or the manganese aluminide particles themselves may also be attacked. The dark areas would then signify sites of preferential dissolution of these particles.

On further raising the controlled potential to -610 mV S.C.E.,

7091 was anodically polarized. The surface of the 7091 sample did not exhibit uniform attack as had been the case when it was cathodically polarized, the protective oxide film being reduced in select areas. In these areas, preferential attack seems to occur at the precipitates and at the grain boundaries. This is evident in Figure 19(c) as an even distribution of small dark areas and the outlining of some grains. These larger dark areas might be attributed to aggregates of precipitates in the grain boundaries.

At the final controlled potential of -500 mV S.C.E., both the X7091 and Al-7.5 a/o Mn have similar corrosion rates: Both have a current density of approximately $20 \mu\text{A}/\text{cm}^2$ (Figure 18). Also, both have similar microstructural characteristics while corroding, exhibiting preferential attack at the sites of the precipitates or particles. The Al-7.5 a/o Mn alloy apparently preferentially corrodes at the manganese aluminide- α aluminum interface. This is signified in Figure 19(f) by the presence of small islands in the size range of the manganese aluminide particles, surrounded by preferential attack of the matrix. The X7091 seems to be preferentially attacked at the precipitates as shown in Figure 19(e).

4.4.3 Galvanic Couple Response

This test was used to examine the effect of coupling the two candidate phases of the proposed duplex alloy, the polarizing current of the samples being measured as a function of time. The micrographs in Figure 21 show that the microstructural characteristics of the corroded X7091 are similar to those of X7091 cathodically polarized at -900 mV S.C.E. The corroded Al-Mn alloy (Figure 21) is similar to Al-7.5 a/o Mn

anodically polarized at the same -900 mV potential. The polarizing current versus time results (Figure 20) showed that over a 20-hour period, the current was generally around 0.25 μ A. The current density at the Al-7.5 a/o Mn electrode is similar to that exhibited while polarizing at -900 mV S.C.E. The low current flow on short-circuiting the X7091/Al-7.5 a/o Mn couple signifies that the X7091 does not, to any great degree, increase the corrosion rate of the Al-7.5 a/o Mn and vice versa.

5.0 CONCLUSIONS AND FUTURE EFFORTS

This initial phase of the program has not only shown that the production of a high modulus, duplex aluminum alloy is feasible, it has also evaluated the principal factors influencing the mechanical response.

The major conclusions derived from the production feasibility study are:

- The high modulus Al-17 w/o Mn alloy powder addition is readily produced using normal air atomization. The $MnAl_6$ aluminide size in this powder is a function of the powder particle size.
- The high modulus powder may be blended in various proportions with 7075 or X7091 and compacted, forged or extruded using conventional powder metallurgy techniques. The resulting duplex alloys have a fully dense microstructure with no evidence of Al-Mn associated cracking or void formation.
- The elongation of the Al-Mn powder particles during processing is not only a function of the reduction ratio during processing, but also the aluminide size within the Al-17 w/o Mn powder.

The novel method used for the manufacture of the duplex alloys can produce a wide range of microstructural characteristics. The effect of these microstructural features on the mechanical response of the

alloys is summarized in Table VI and itemized below.

- Decreasing the powder size, or increasing the cooling rate, decreases the aluminide size in the Al-17 w/o Mn powder. This endows inherently better mechanical properties to the powder and enhances its elongation.
- Increasing the volume fraction of the high modulus powder increases the modulus of the resulting duplex alloy. This improvement, however, is at the expense of ductility and ultimate strength. In these initial alloys, the optimum addition level was found to be 20 v/o.
- Increasing the reduction ratio during direct powder consolidation improves the interparticle bonding and increases the elongation of the Al-17 w/o Mn powder particles, hence improving the modulus, strength and ductility of the duplex alloy.

Thus, these experiments have established firm guidelines for property optimization of the duplex alloys being produced and may be summarized as follows:

- i) A fine Al-17 w/o Mn powder is preferred.
- ii) A high reduction ratio during consolidation is desirable.
- iii) With the initial alloys, a balance between optimum modulus, ductility and strength was attained at 20 v/o addition of Al-Mn. The

use of a finer Al-17 w/o Mn powder may achieve acceptable ductility at higher volume fractions.

The corrosion properties of the individual components of the duplex alloy have been investigated. The initial results indicate:

- A 20 v/o addition of Al-Mn tends to cathodically polarize X7091 or 7075 as shown in the controlled potential corrosion and galvanic couple tests.
- In comparison to 7075, the X7091 does not appear to increase the rate of dissolution of the Al-Mn.

REFERENCES

1. W. L. Otto, "Metallurgical Factors Controlling Structure in High Strength P/M Products", AFML TR-76-60, May 1976.
2. W. S. Cebulak in Rapid Solidification Processing, Principles and Technologies, Claitor Publishing (1978), Baton Rouge, La.
3. T. H. Sanders, Factors Influencing Toughness and Other Properties of Aluminum Lithium Alloys, NADC Contract #N62269-76C-0271, June 14, 1979.
4. R. E. Sanders, Jr., G. J. Hildeman and D. J. Lage, Elevated Temperature Alloy Development, AFML Contract #F33615-77-C-5086, March 31, 1979.
5. Proc. Rapid Solidification Processing, 1977, Eds. R. Mehrabian et al, Claitor's Publ. Div., Baton Rouge, La.
6. Proc. 2nd Intern'l Conf. on Rapid Solidification, 1980, Eds. R. Mahrabian et al, Claitor's Publ. Div., Baton Rouge, La.
7. Third Intern'l Conf. on Rapidly Quenched Metals, III, Ed. B. Cantor, The Metals Society, London.
8. V. S. Agarwala and Y. V. Murty, A Controlled-Potential Corrosion Study of Al-4.5 Cu Alloy in 3.5% NaCl Solution, Metallography, 10, (1977), pp. 451-460.
9. J. Gurland, An Approximate Method for the Estimate of the Contribution of Load Transfer to the Internal Stress in Dispersed Particles, Scripta, 13, (1979), pp. 967-969.
10. J. Gurland, A Structural Approach to the Yield Strength of Two-Phase Alloys with Coarse Microstructures, Materials Sci. and Eng., 40 (1979), pp. 59-71

TABLE I
CHEMICAL COMPOSITIONS FOR ALLOYS

(weight percent)

Alloy	Si	Fe	Cu	Mn	Mg	Cr	Zn	Co	Ti
7075	0.40	0.50	1.2 - 2.0	0.30	2.1 - 2.9	0.18 - 0.28	5.1 - 6.1		0.20
X7091	0.12	0.15	1.1 - 1.8	--	2.0 - 3.0	--	5.8 - 7.1	0.20 - 0.60	--
Al-Mn	--	--	--	17.0	--	--	--	--	--

Balance Aluminum

TABLE II

EXTRUSION PARAMETERS

Preheat Temperature: 390 - 400°C (734 - 752°F)

Extrusion Temperature: 400°C (750°F)

Initial Area: $2.0 \times 10^3 \text{ mm}^2$ (3.14 in²)

<u>Alloy</u>	<u>Form</u>	<u>Extrusion Speed</u>	<u>Upset Load*</u>	<u>Running Load*</u>	<u>Reduction</u>
7075	Preform	25 ipm	156 tons	150 tons	20/1
X7091	Preform	25 ipm	235	175	20/1
7075+20 ^V / _o Al-17 ^W / _o Mn	Preform	25 ipm	275	200	20/1
X7091+20 ^V / _o Al-17 ^W / _o Mn	Preform	25 ipm	250	185	20/1
7075+20 ^V / _o Al-17 ^W / _o Mn	Direct Powder	25 ipm	200	180	20/1
X7091+20 ^V / _o Al-17 ^W / _o Mn	Direct Powder	25 ipm	235	192	20/1

*Conversion: tons to kg, multiply by 9.0718×10^2

TABLE III
TENSILE TEST DATA FOR DUPLEX ALLOYS IN THE T-6 CONDITION

Alloy + Processing	E		σ_{UTS}		% RA Reduction in Area %	Impact Strength	
	10 ⁶ Psi (GPa)	ksi (MPa)	ksi (MPa)	ft-lb (J)			
7075							
2:1 forge	---	---	---	---	---	---	---
7:1 forge	9.60	(66.2)	85.0	(586)	36.5	4.5	(6.1)
7:1 forge + coarsen	---	---	85.2	(587)	34.4	4.0	(5.4)
20:1 extrusion	9.55	(65.8)	98.5	(678)	18.7	---	---
7075+10 ^V /o Al-17 ^W /o Mn							
2:1 forge	9.52	(65.6)	---	---	< 1	1.5	(2.0)
7:1 forge	10.74	(74.0)	74.5	(514)	2.1	3.0	(4.1)
7:1 forge + coarsen	---	---	71.8	(495)	2.4	1.5	(2.0)
20:1 extrusion	---	---	---	---	---	---	---
7075+20 ^V /o Al-17 ^W /o Mn							
2:1 forge	10.05	(69.3)	60.0	(414)	< 1	1.7	(2.3)
7:1 forge	10.58	(72.9)	68.9	(475)	< 1	2.0	(2.7)
7:1 forge + coarsen	---	---	67.7	(467)	< 1	1.5	(2.0)
20:1 extrusion	11.60	(80.0)	72.0	(496)	< 1	---	---
7075+40 ^V /o Al-17 ^W /o Mn							
2:1 forge	12.49	(86.1)	45.0	(310)	< 1	1.5	(2.0)
7:1 forge	11.16	(76.9)	67.9	(468)	< 1	1.0	(1.4)
7:1 forge + coarsen	---	---	61.0	(420)	< 1	1.0	(1.4)
20:1 extrusion	---	---	---	---	---	---	---
X7091							
20:1 extrusion	8.82	(60.8)	90.9	(627)	30.6	---	---
X7091+20 ^V /o Al-17 ^W /o Mn							
20:1 extrusion	10.88	(75.0)	73.0	(503)	< 1	---	---

TABLE IV

TENSILE TEST DATA FOR DUPLEX ALLOYS* IN THE 0 TEMPER AND T-6 CONDITION

Alloy	Temper	E		σ_{YS}		σ_{UTS}		% RA	% EL
		Elastic Modulus 10 ⁶ Psi (GPa)	Yield Strength ksi (MPa)	Yield Strength ksi (MPa)	Ultimate Strength ksi (MPa)	Ultimate Strength (MPa)	Reduction in Area		
7075	0	10.2 (70.3)	20.9 (144)	43.2 (299)	33	18.4			
	T-6	10.5 (72.4)	87.0 (600)	94.8 (654)	17.1	10.4			
7075+20 ^V /o Al-17 ^W /o Mn	0	11.2 (77.2)	22.4 (154)	34.7 (239)	8.8	5.3			
	T-6	11.7 (80.7)	68.3 (471)	70.7 (487)	1.9	< 1			
X7091	0	10.2 (70.3)	20.3 (140)	42.1 (290)	49.5	21.4			
	T-6	10.3 (71.0)	82.8 (571)	86.5 (596)	41.8	13.5			
X7091+20 ^V /o Al-17 ^W /o Mn	0	-----	24.0 (165)	34.8 (240)	8.4	6.6			
	T-6	11.5 (79.3)	71.9 (496)	71.9 (496)	1.2	< 1			

* Direct powder extrusions 20:1

TABLE V

SHORT TERM OPEN CIRCUIT POTENTIAL TEST DATA*

Average Open Circuit Potential	X7091	Al-7.5 ^a /o Mn
		-840 mV S.C.E.
		-906 mV S.C.E.

*This is a weighted average.

TABLE VI
SUMMARY OF PROCESSING PARAMETER/PROPERTY RELATIONS

<u>Duplex Alloy Addition Parameter</u>	<u>Size</u>	<u>V_f</u>	<u>% Mn</u>	<u>% D</u>	<u>Modulus</u>	<u>Strength</u>	<u>Ductility</u>	<u>Hardness</u>
Powder Size	↗	↖	↖	↖	↖	↖	↖	—
Volume Fraction	↖	↗	↖	↖	↖	↗	↗	↖
Manganese Content	↖	↖	↖	↖	↖	↖/↗	↖	↖
Degree of Deformation	↖	↖	↖	↖	↖	↖	↖	—

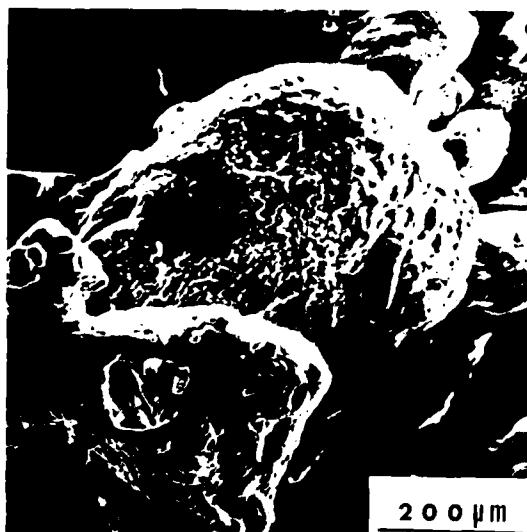
↖ Property Improvement
 ↗ Property Degradation
 ↖/↗ Dependent on interplay of S, V_f , % Mn, % D
 — No Change



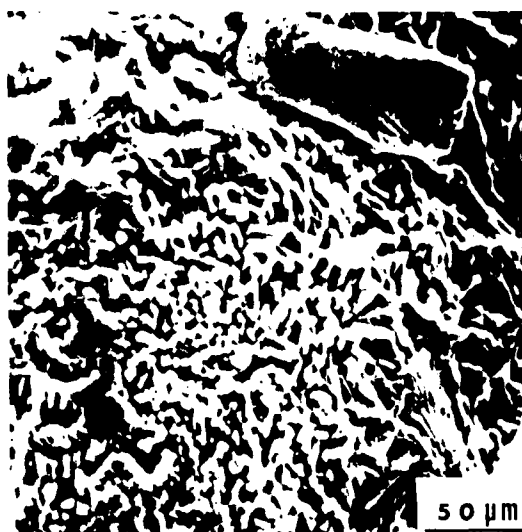
a)



b)



c)

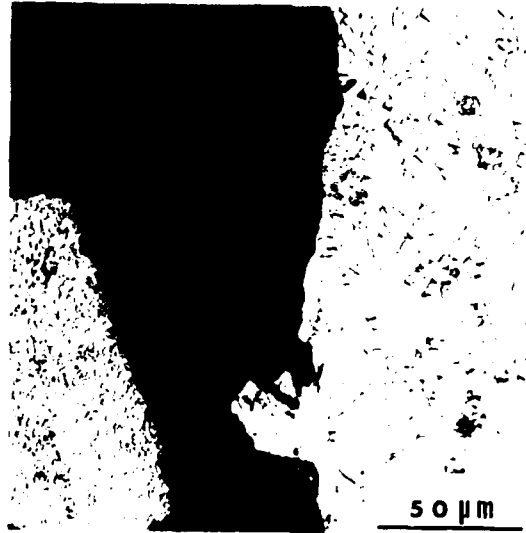


d)

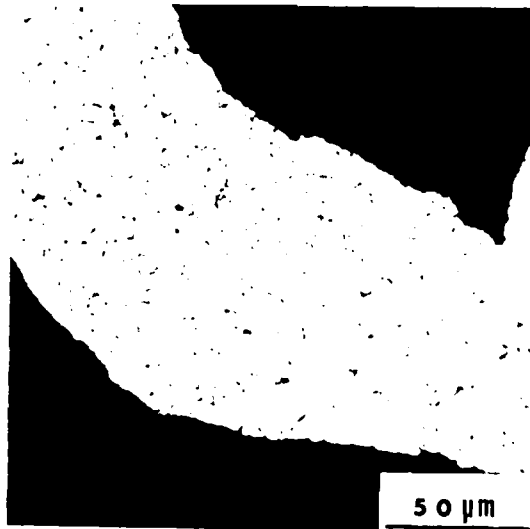
Figure 1. Scanning electron micrographs of as-atomized powder

a) 7075
b) 7075

c) Al-17 w/o Mn
d) Al-17 w/o Mn



a)



b)

Figure 2. As-atomized

- a) Al-17 w/o Mn powder
- b) Al-Zn-Mg (7075) powder (Keller's reagent)

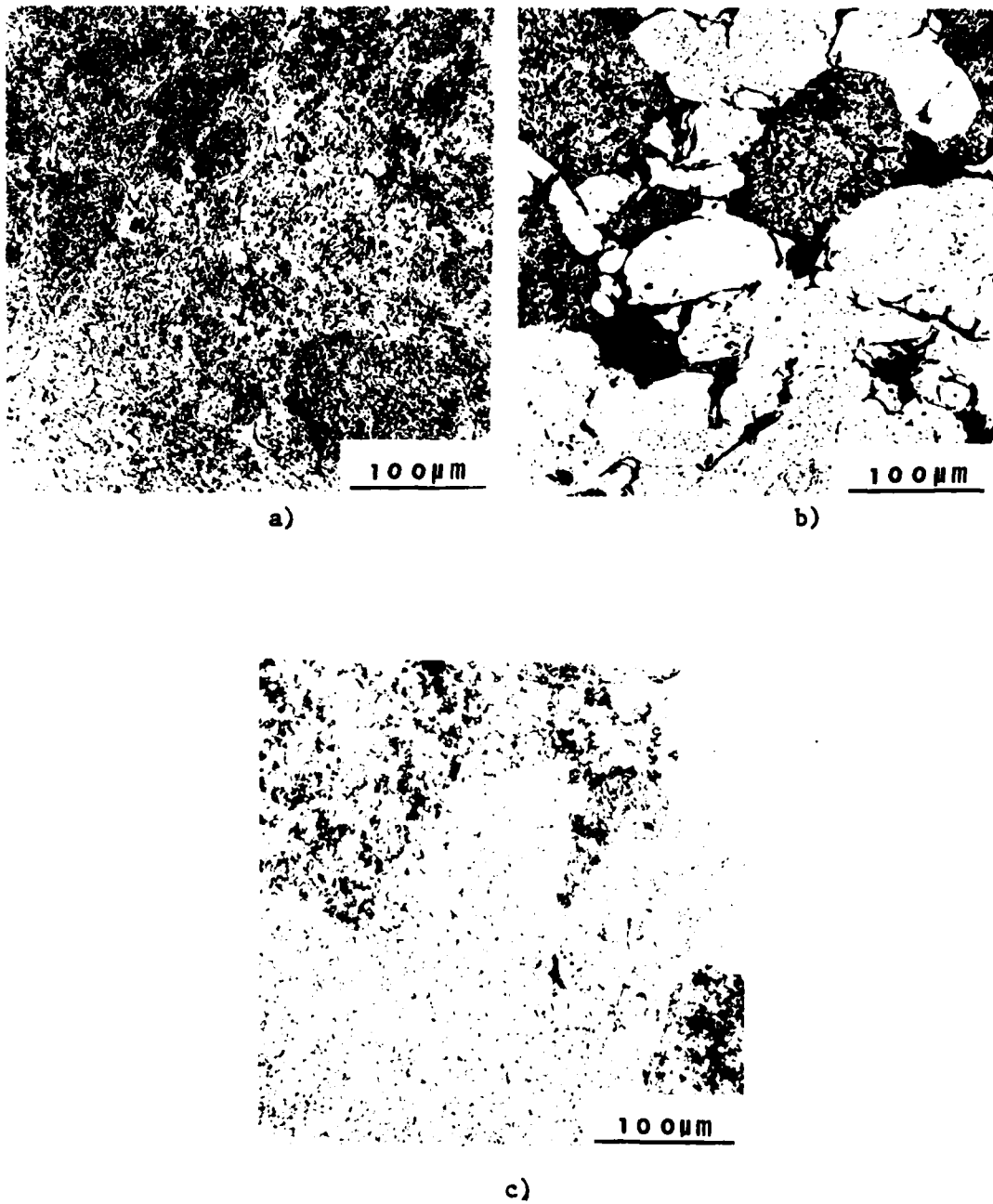


Figure 3. Vacuum hot pressed 538°C (1000°F)

- a) 7075
- b) 7075 + 10 v/o (Al-17 w/o Mn)
- c) 7075 + 20 v/o (Al-17 w/o Mn)

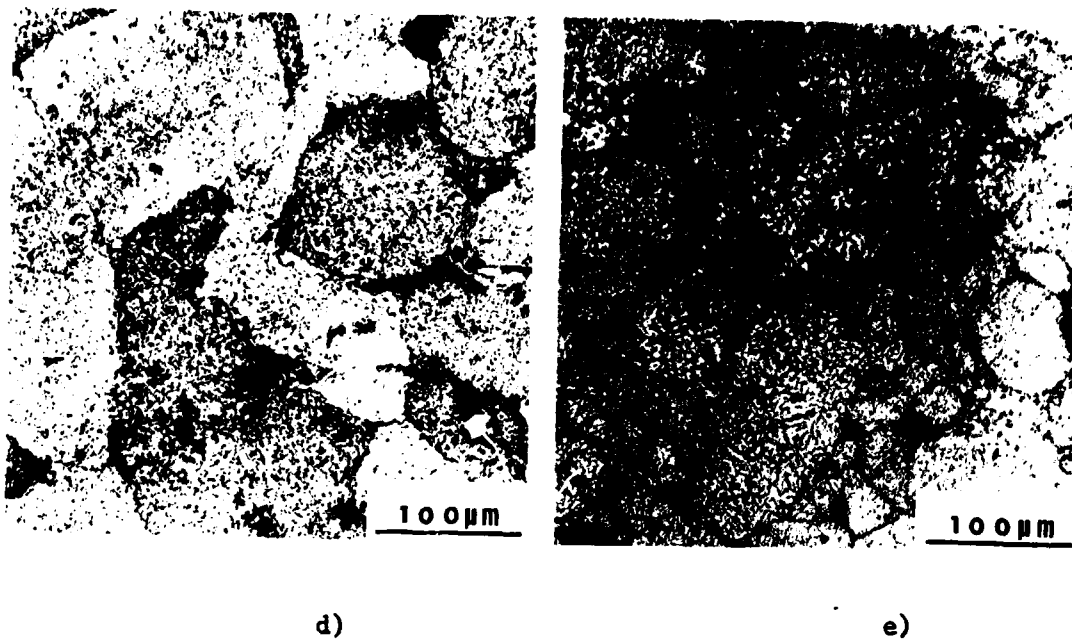


Figure 3. Vacuum hot pressed 538°C (1000°F)

- d) 7075 + 40 v/o (Al-17 w/o Mn)
- e) 100% Al-17 w/o Mn (Keller's reagent)

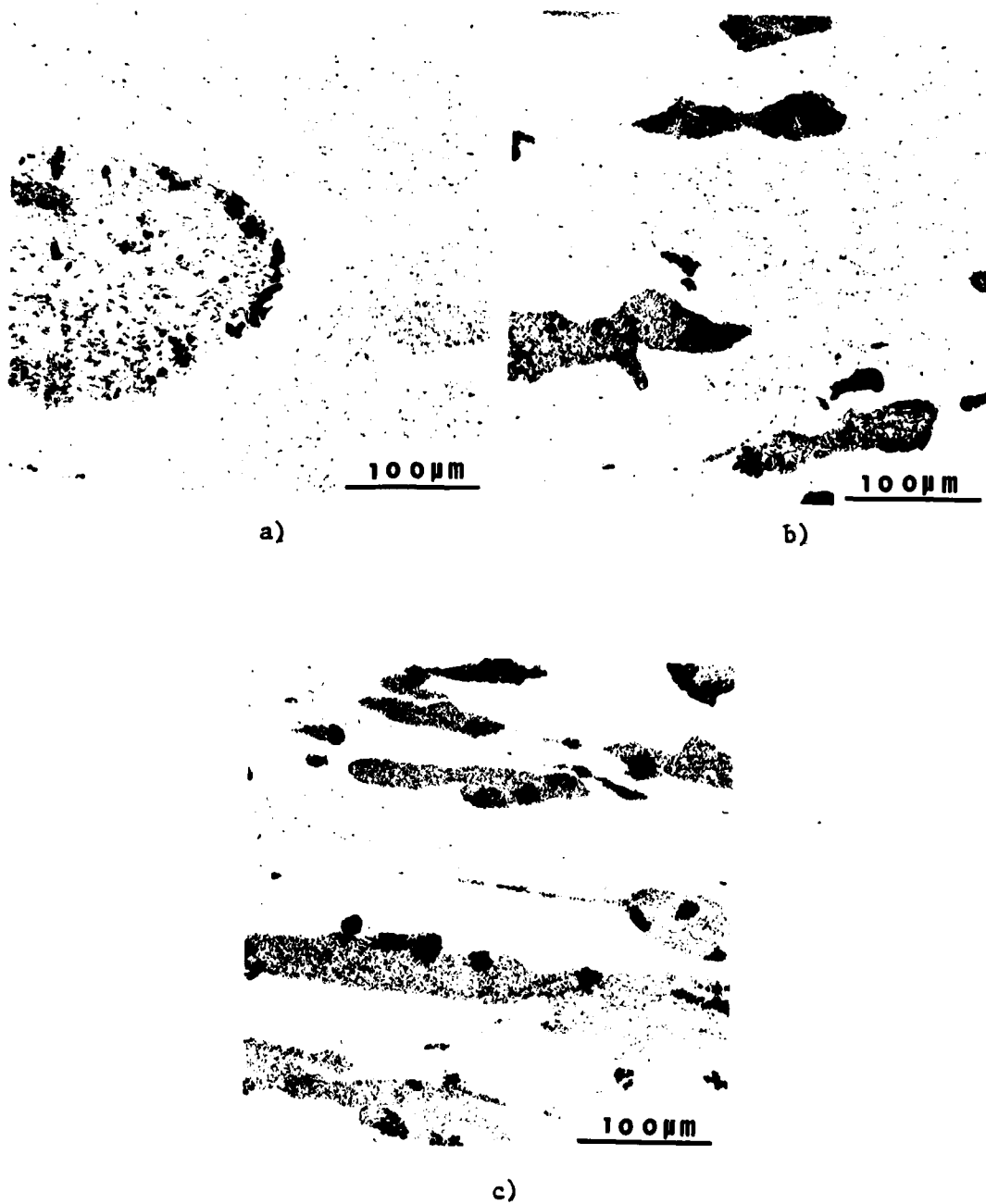


Figure 4. Vacuum hot pressed 538°C (1000°F) and upset forged to a reduction in height of 2:1

- a) 7075 + 10 v/o (Al-17 w/o Mn)
- b) 7075 + 20 v/o (Al-17 w/o Mn)
- c) 7075 + 40 v/o (Al-17 w/o Mn) (Keller's reagent)

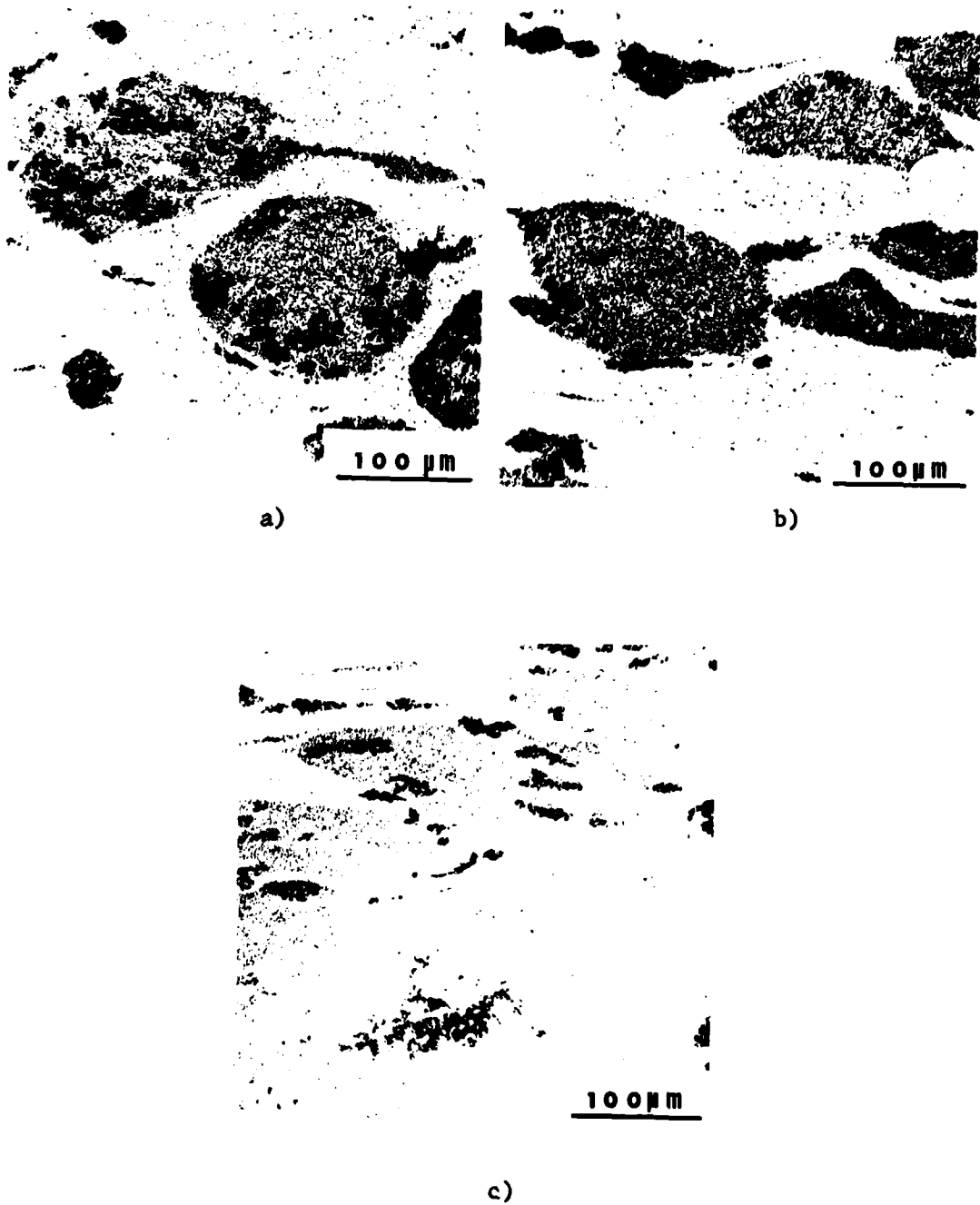


Figure 5. Vacuum hot pressed 538°C (1000°F) and upset forged 480°C (896°F) to a reduction in height of 7:1

- a) 7075 + 10 v/o (Al-17 w/o Mn)
- b) 7075 + 20 v/o (Al-17 w/o Mn) (Keller's reagent)
- c) 7075 + 40 v/o (Al-17 w/o Mn) (Keller's reagent)

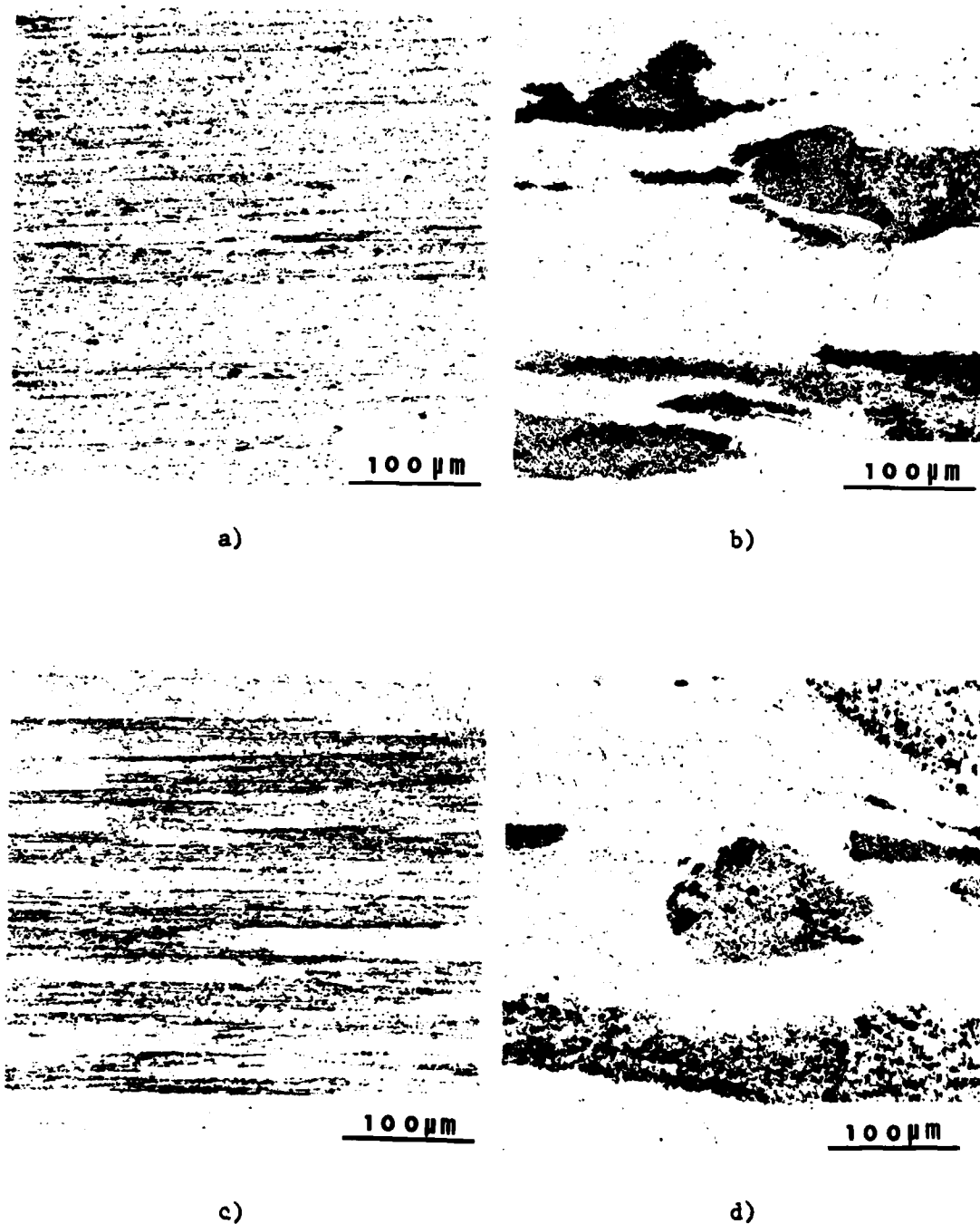
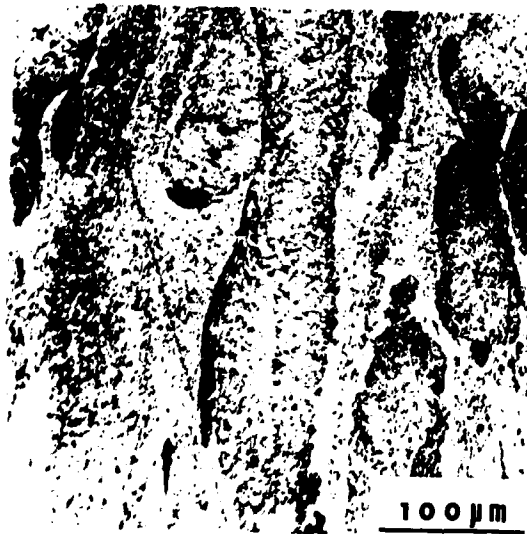
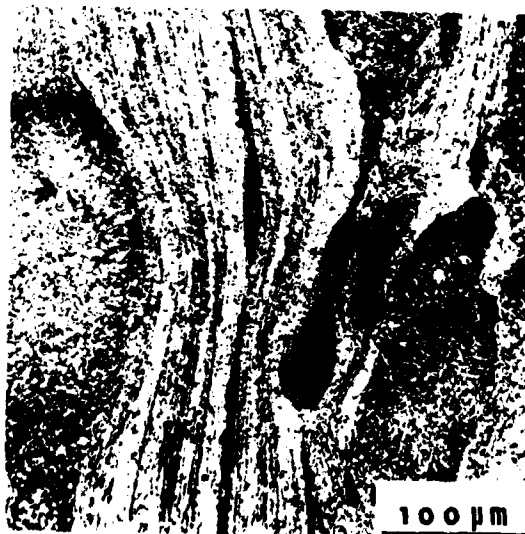


Figure 6. Vacuum hot pressed 538°C (1000°F) billet extrusion 400°C (752°F) to a reduction in cross-sectional area of 16:1

- a) 7075
- b) 7075 + 20 v/o (Al-17 w/o Mn)
- c) Al-Zn-Mg (X7091)
- d) X7091 + 20 v/o (Al-17 w/o Mn) (Graff-Sargent reagent)



a)



b)

Figure 7. Direct powder extrusion 390°C (735°F) to a reduction in cross-sectional area of 20:1

a) 7075 + 20 v/o (Al-17 w/o Mn)

b) X7091 + 20 v/o (Al-17 w/o Mn) (Graff-Sargent reagent)

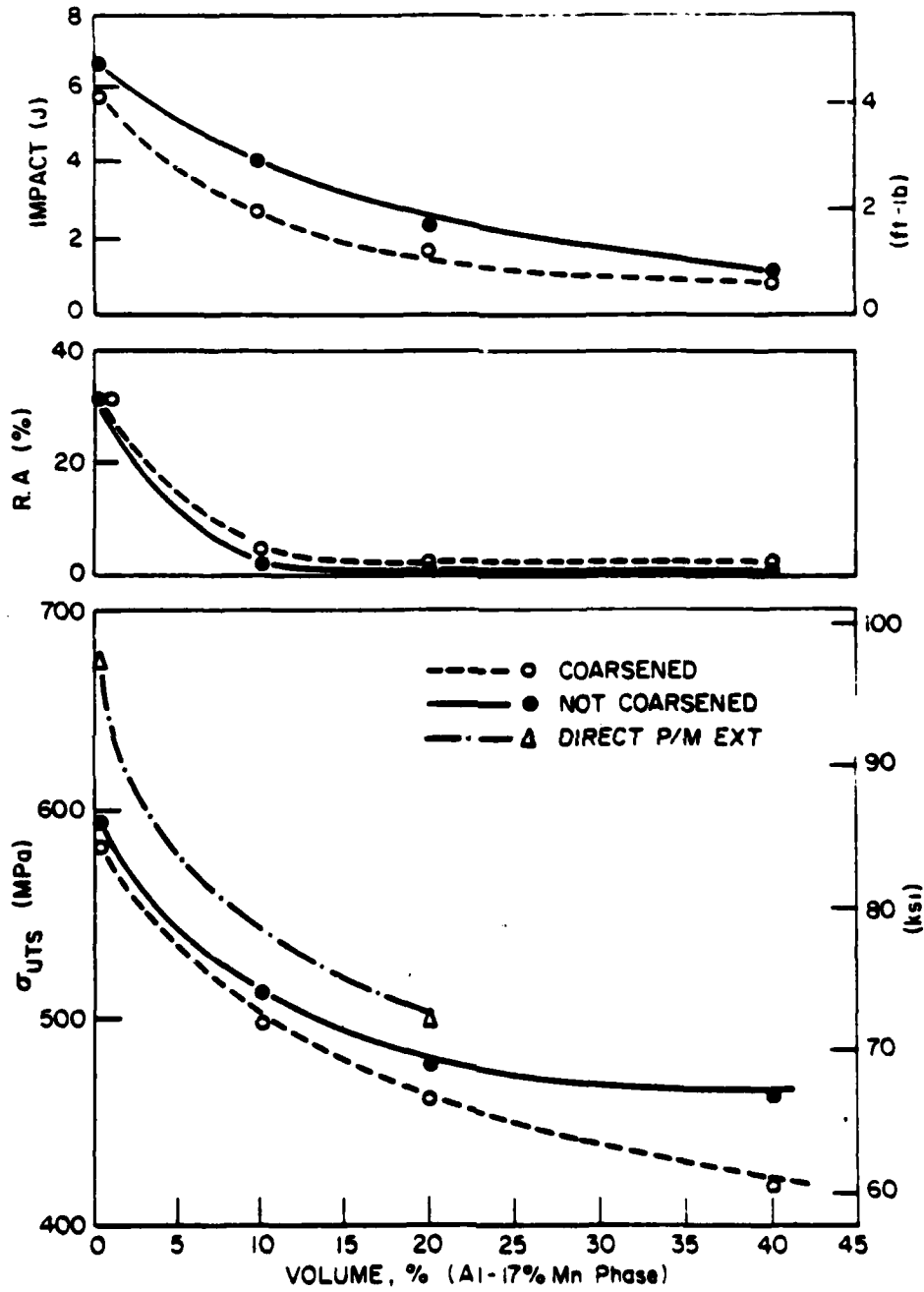


Figure 8. Impact strength, reduction in cross-sectional area, and ultimate tensile strength versus the volume percent of Al-17 w/o Mn.

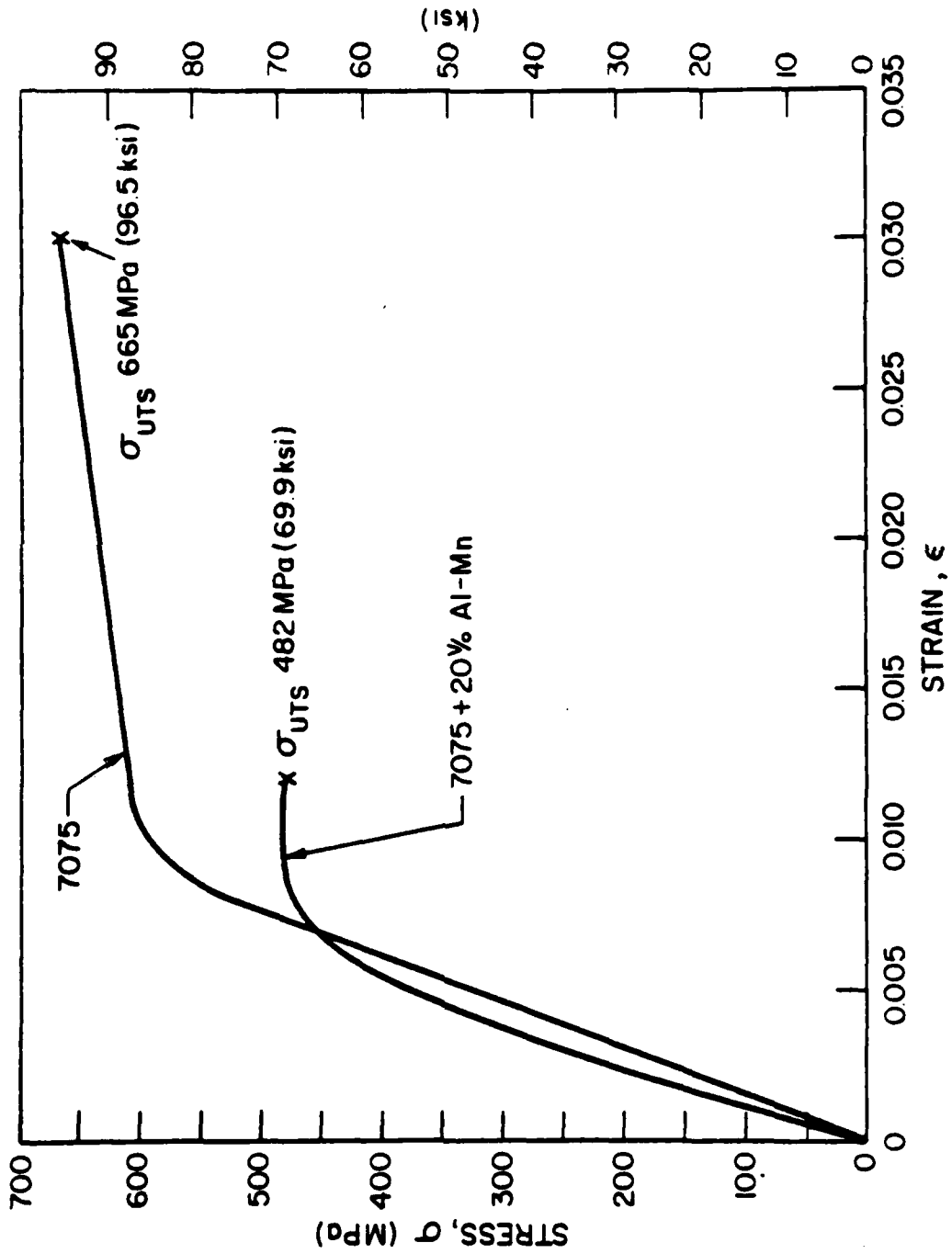


Figure 9. Stress-strain response of direct powder extruded, 390°C (735°F), 7075 and 7075 + 20 v/o (Al-17 w/o Mn), 20:1 reduction in cross-sectional area.

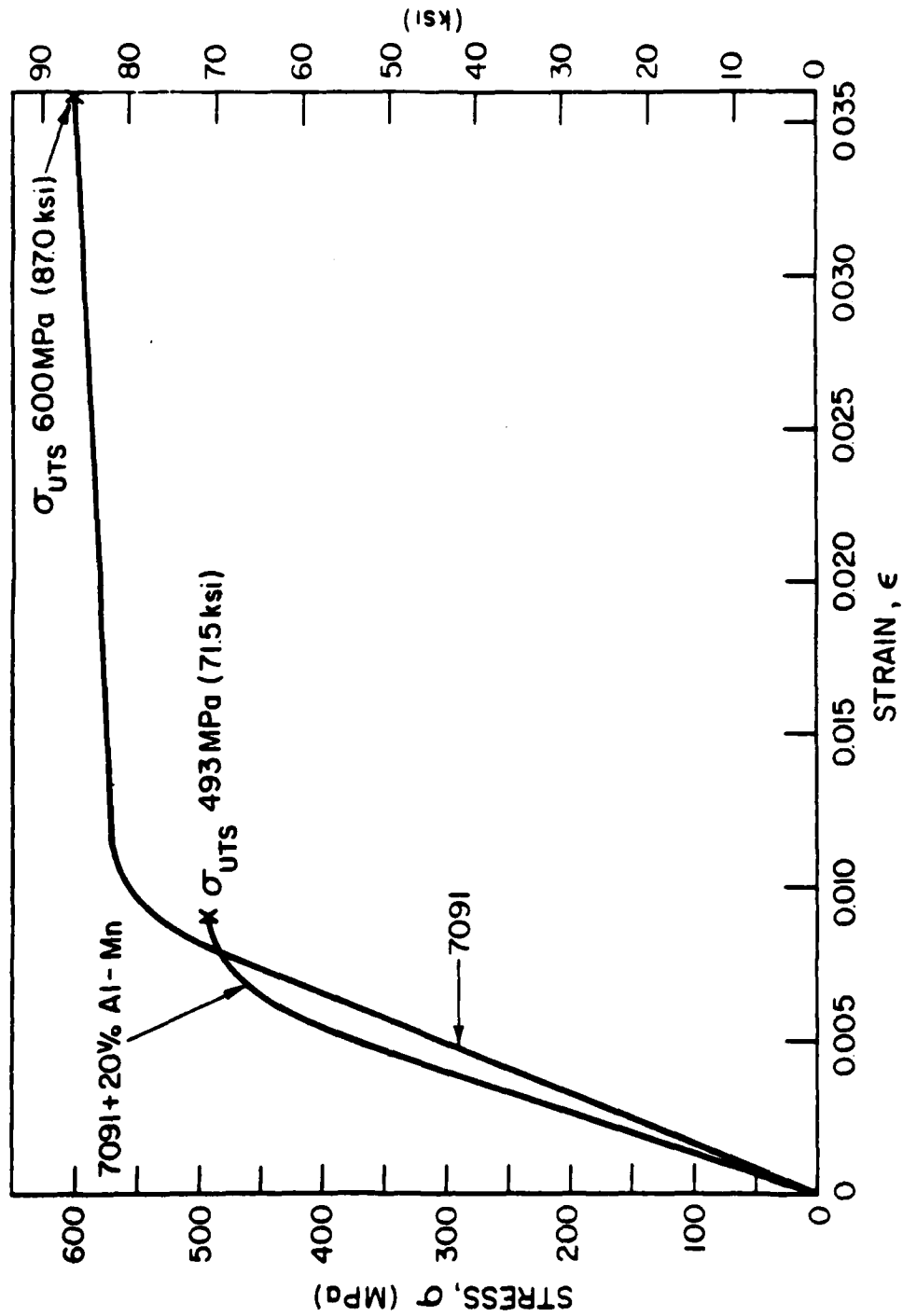


Figure 10. Stress-strain response of direct powder extruded, 390°C (735°F), X7091 and X7091 + 20 v/o (Al-17 w/o Mn), 20:1 reduction in cross-sectional area.

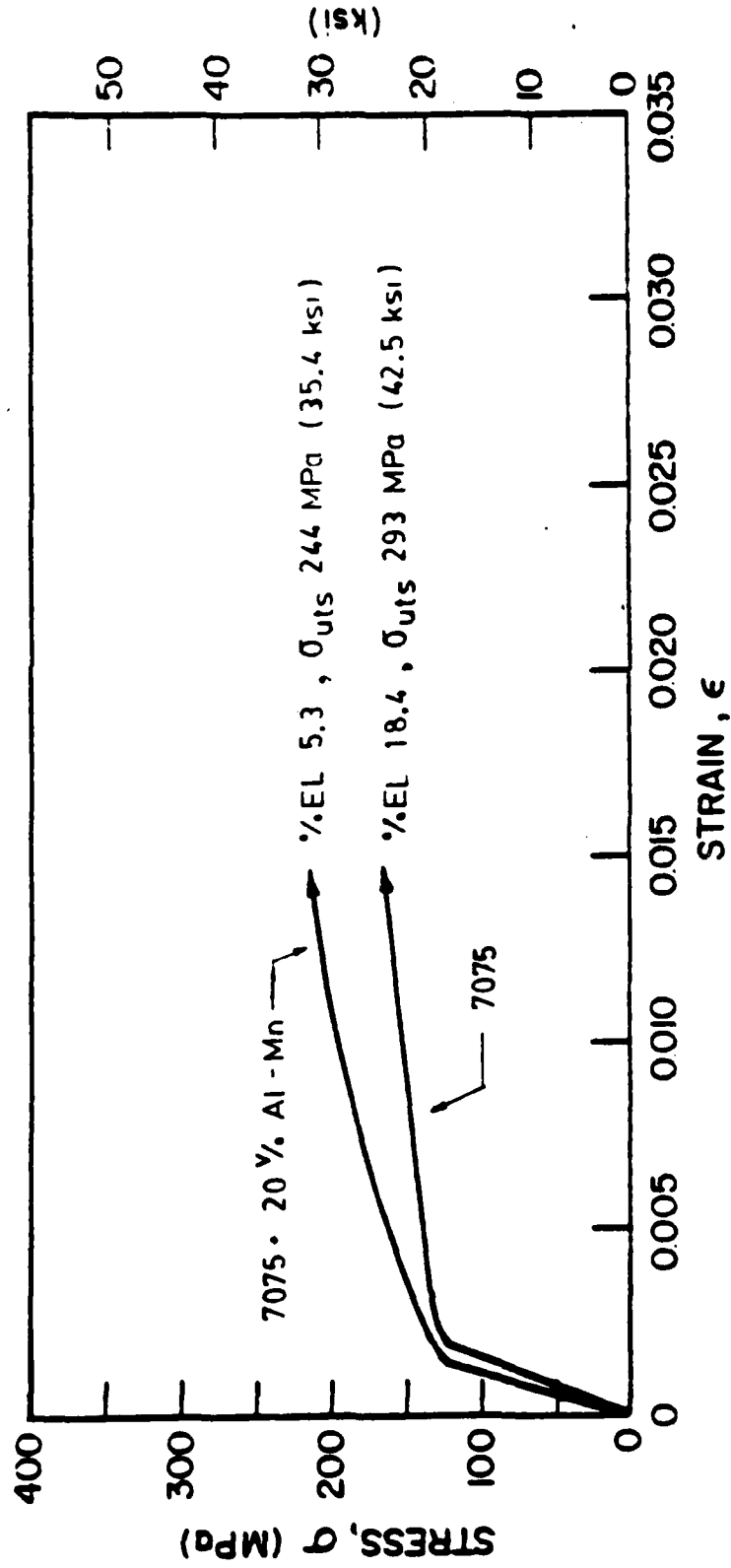


Figure 11. Stress-strain response of direct powder extruded, 390°C (735°F), 0 temper, 7075 and 7075 + 20 V/o (Al-17 w/o Mn), 20:1 reduction in cross-sectional area.

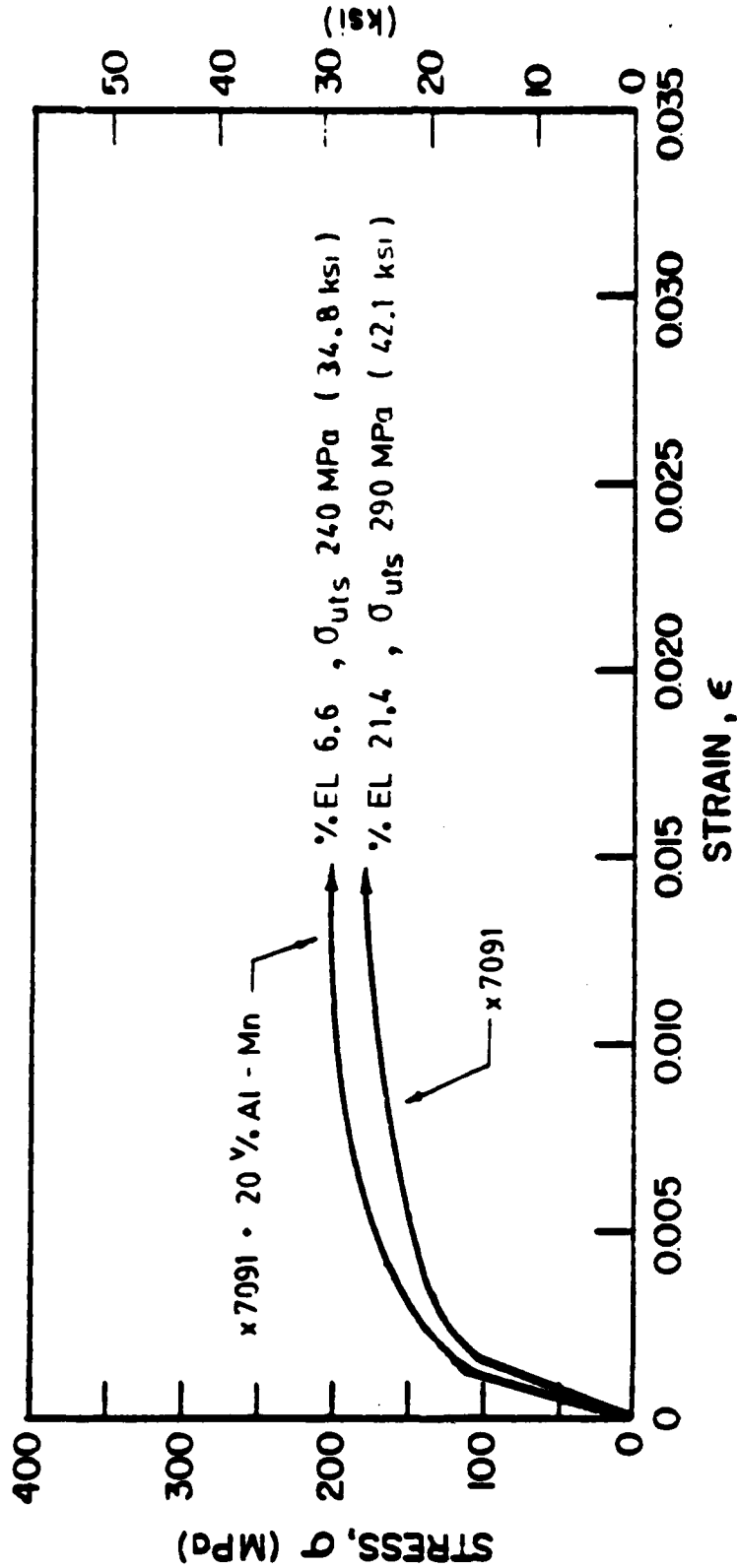


Figure 12. Stress-strain response of direct powder extruded, 390°C (735°F), 0 temper X7091 and X7091 + 20 v/o (Al-17 w/o Mn).

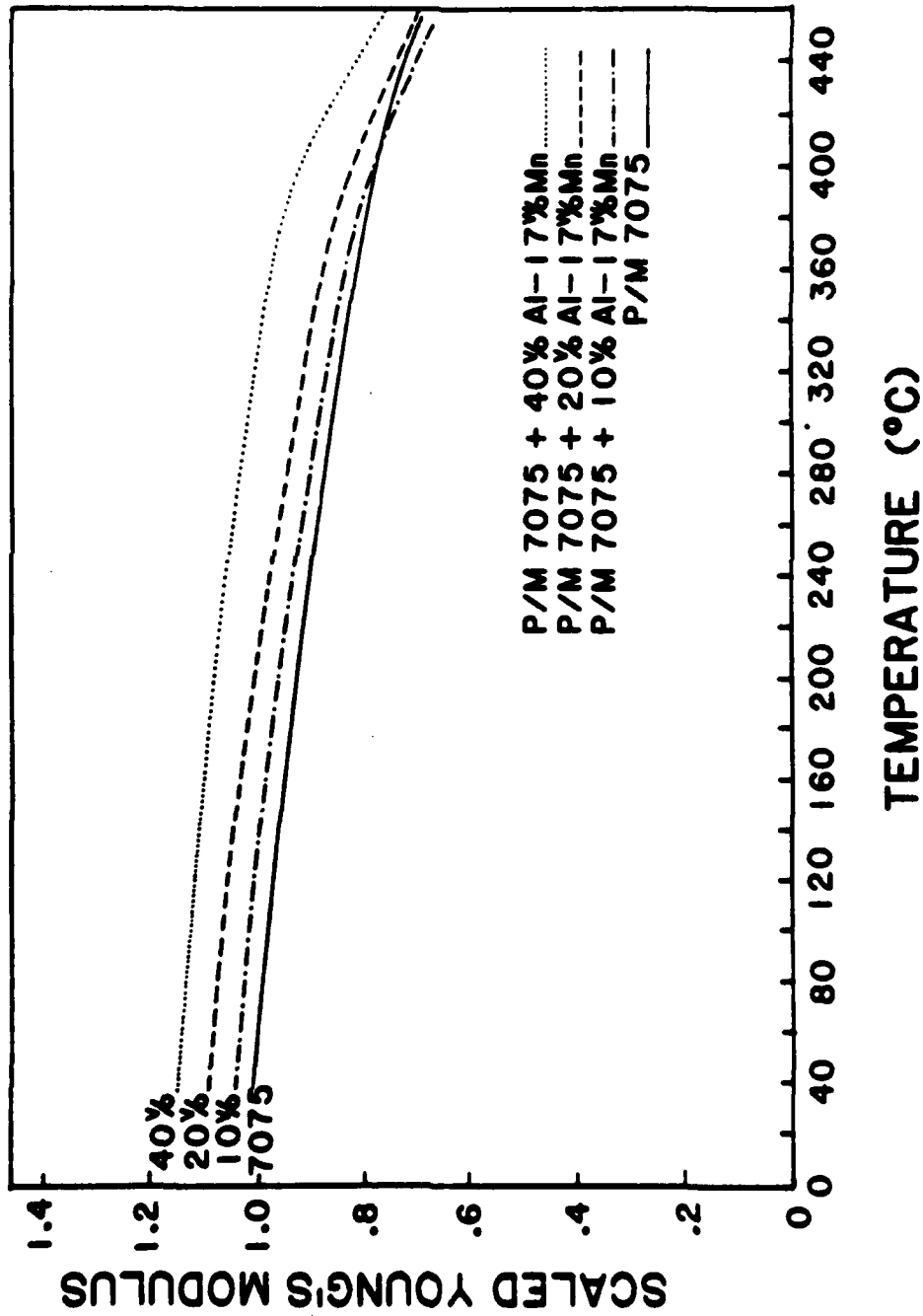
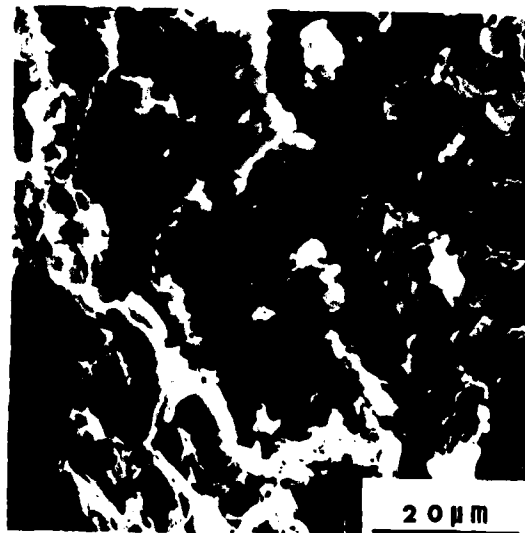


Figure 13. Normalized Young's modulus versus temperature for 7075 with varying amounts of the Al-17 w/o Mn addition.



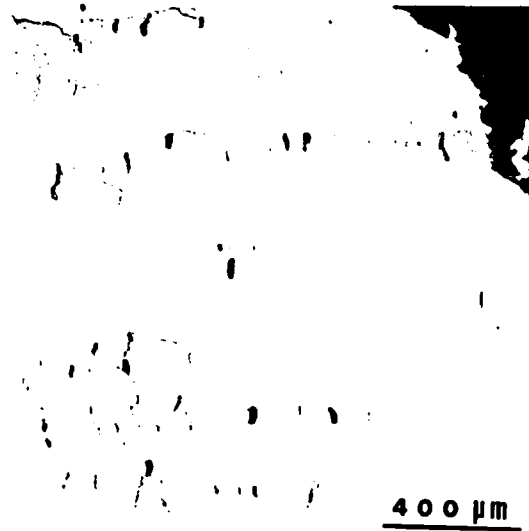
a)



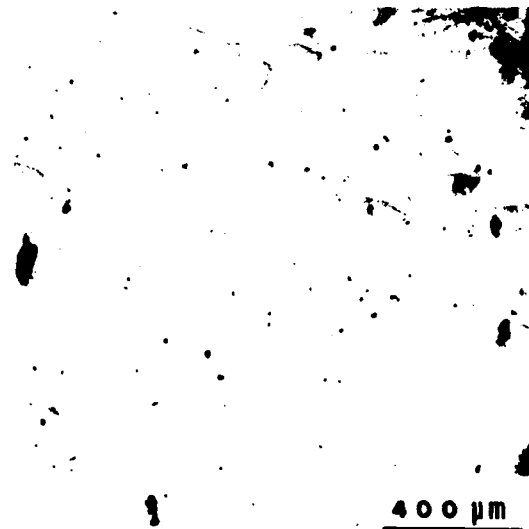
b)

Figure 14. Impact fracture surface of hot upset forged 480°C (896°F) to a reduction in height of 7:1.

- a) 7075 + 40 v/o (Al-17 w/o Mn)
- b) Same as (a), but at a higher magnification.



a)



b)

Figure 15. Evidence of plastic-strain incompatibility between the matrix and the Al-17 ^{w/o} Mn addition.

- a) 0 temper 7075
- b) 0 temper 7091

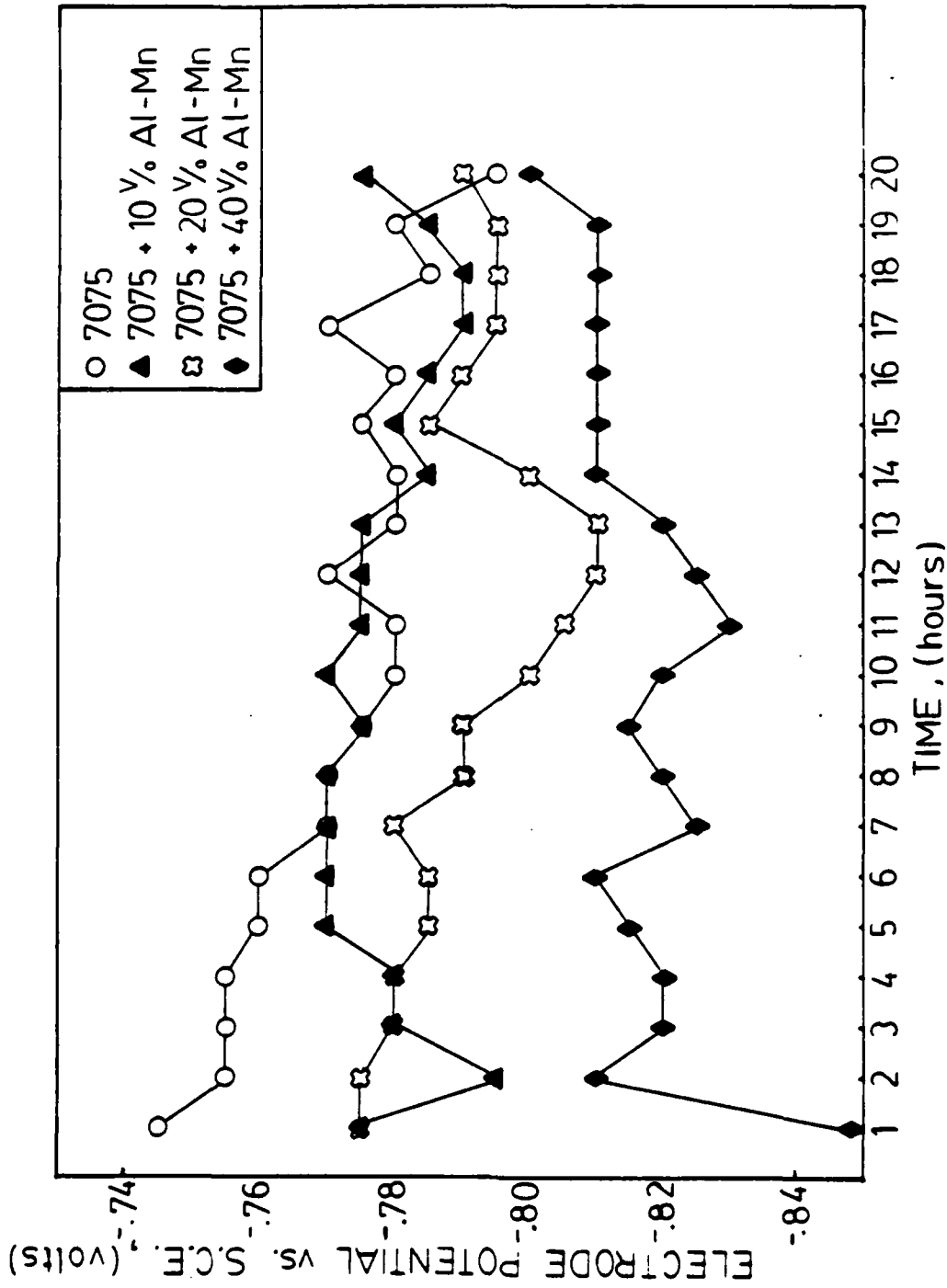
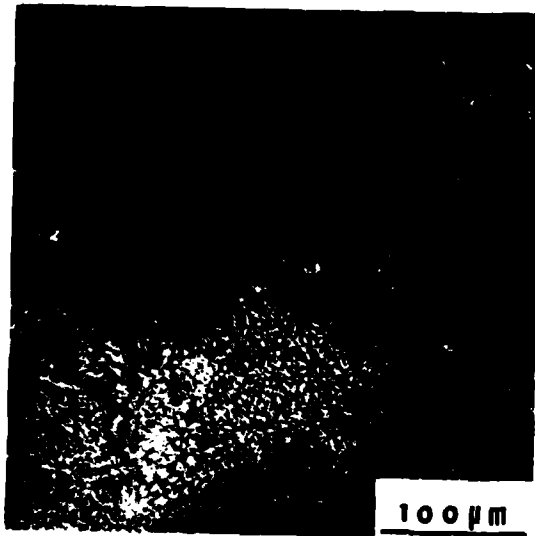


Figure 16. Electrode potential (with a saturated calomel reference) versus time for 7075, 7075 + 10 v/o (Al-17 w/o Mn), 7075 + 20 v/o (Al-17 w/o Mn) and 7075 + 40 v/o (Al-17 w/o Mn).



a)



b)

Figure 17. Microstructural results from the electrode potential test

- a) 7075 + 20 V/o (Al-17 W/o Mn) prior to testing
- b) 7075 + 20 V/o (Al-17 W/o Mn) after electrode potential testing (unetched condition).

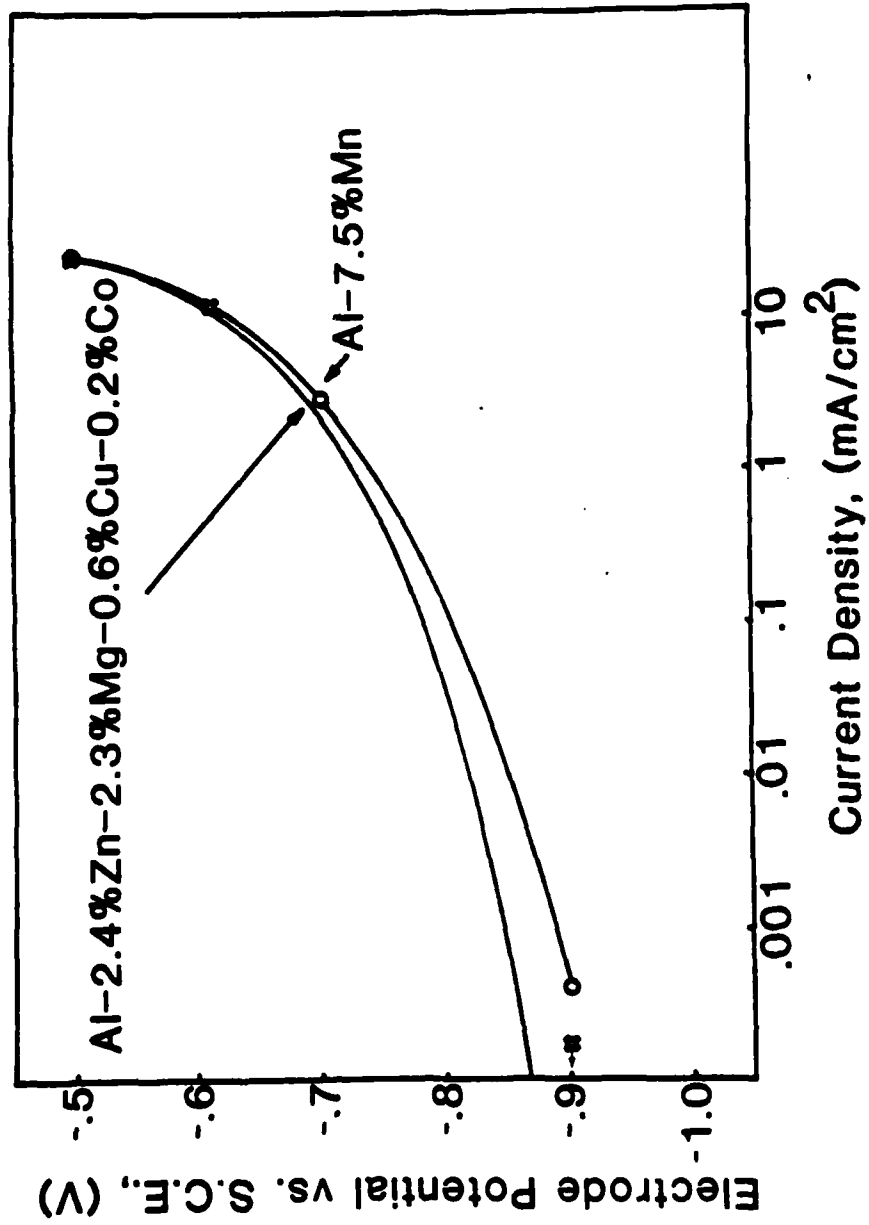


Figure 18. Anodic polarization curve for the X7091 alloy and the Al-7.5 a/o Mn alloy.

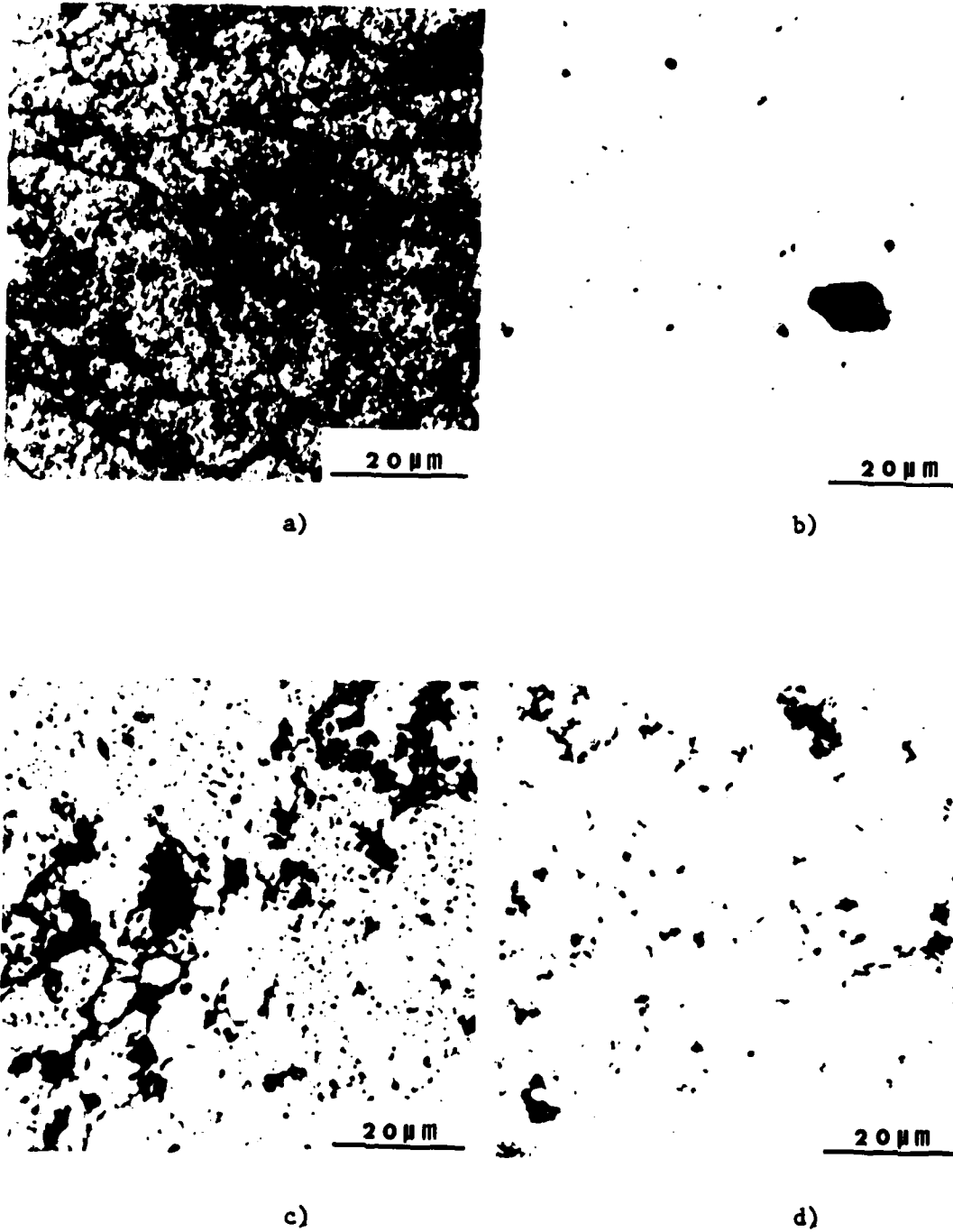
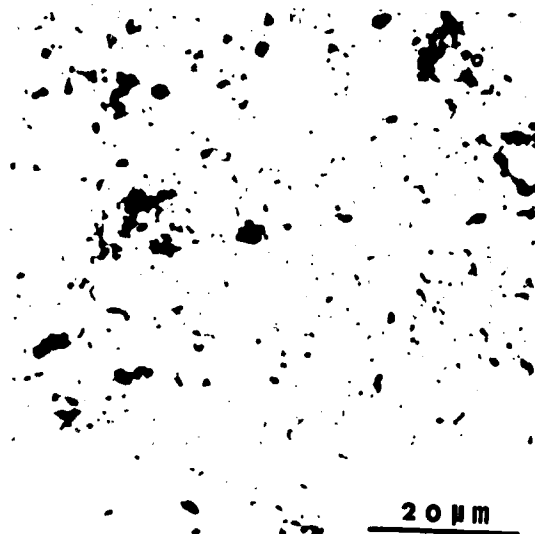


Figure 19. Microstructural results of the X7091 and the Al-7.5 a/o alloy Mn from the three electrode, potentiostatic, controlled-potential corrosion test.

Potential:

- | | |
|-------------------------------|-------------------------------|
| a) E = -900 mV, X7091 | c) E = -610 mV, X7091 |
| b) E = -900 mV, Al-7.5 a/o Mn | d) E = -700 mV, Al-7.5 a/o Mn |



e)



f)

Figure 19. Microstructural results of the X7091 and the Al-7.5 a/o alloy Mn from the three electrode, potentiostatic, controlled-potential corrosion test.

Potential:

- e) E = -500 mV, X7091
- f) E = -500 mV, Al-7.5 a/o Mn

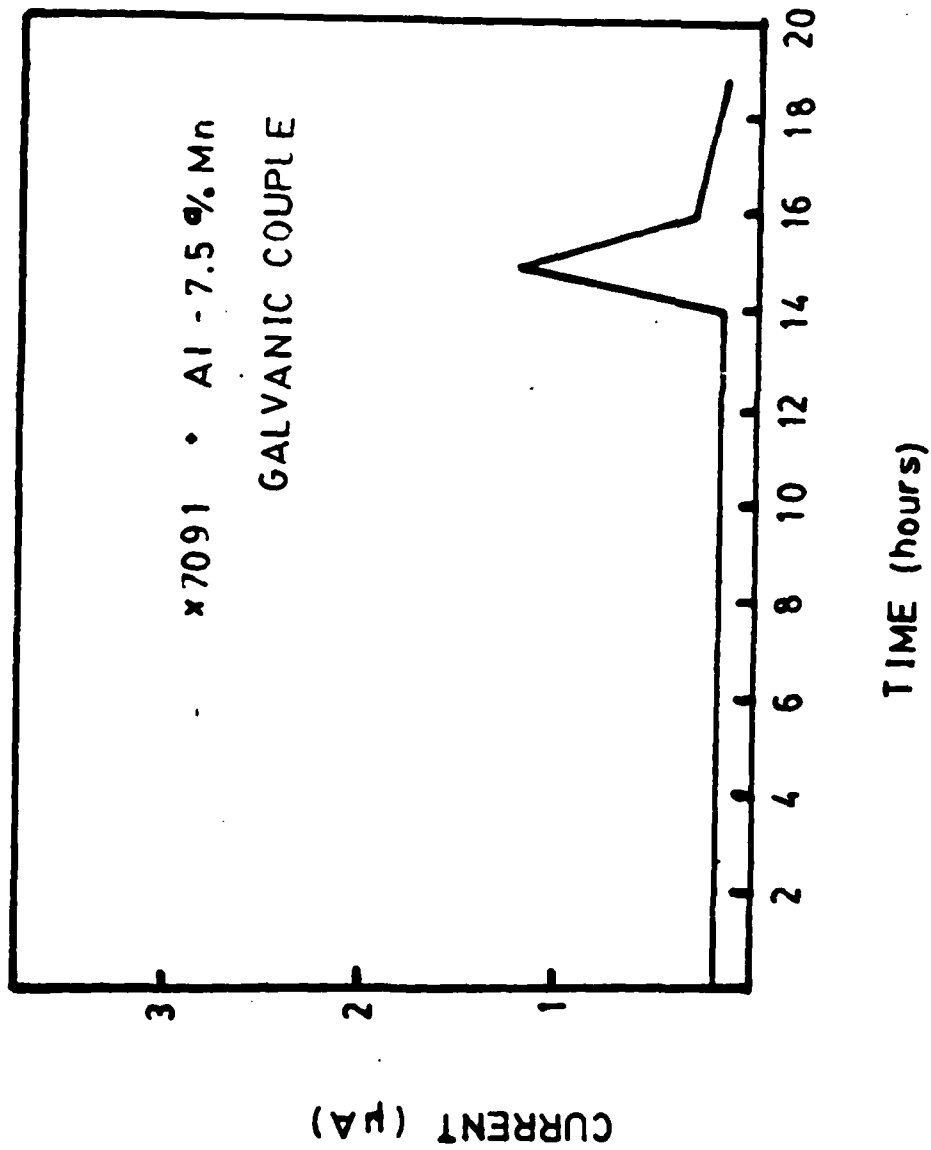
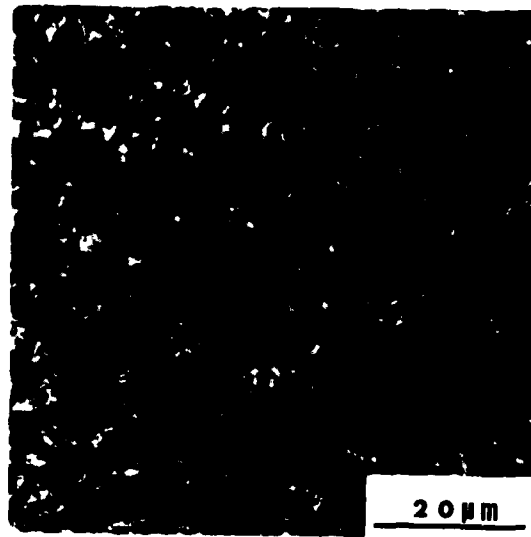


Figure 20. Polarization current versus time for galvanic couple of X7091 immersed in 3.5% NaCl solution opposite sample of Al-7.5 a/o Mn.



a)



b)

Figure 21. Microstructural corrosion couple results.
The surface area ratio was 4:1.

- a) X7091
- b) Al-7.5 a/o Mn (unetched condition)

DISTRIBUTION LIST

Naval Air Systems Command (5)
 Attn: Code AIR-5163D3
 Washington, DC 20361

Office of Naval Research (1)
 Attn: Code 472
 Washington, DC 20350

Office of Naval Research (1)
 495 Summer Street
 Boston, MA 02210
 Attn: Dr. L. H. Peebles

Naval Research Laboratory (2)
 Codes 6306 and 6120
 Washington, DC 20350

Naval Ordnance Laboratory (1)
 Code 234
 White Oak, Silver Spring, MD 20910

Air Force Materials Laboratory (5)
 Wright-Patterson Air Force Base
 Dayton, OH 45433
 Attn: Codes LC 1
 LN 1
 LTF 1
 LAE 1
 MBC 1

Air Force Flight Dynamics Laboratory (1)
 Wright-Patterson Air Force Base
 Dayton, OH 45433
 Attn: Code FDTG

Defense Ceramic Information Center (1)
 Battelle Memorial Institute
 505 King Avenue
 Columbus, OH 43201

Illinois Institute of Technology (1)
 Research Institute
 10 West 35th Street
 Chicago, IL 60616
 Attn: Dr. E. Hofer

Brunswick Corporation (1)
 Technical Products Division
 325 Brunswick Lane
 Marion, VA 24354

Acurex
 Aerospace Systems Division
 485 Clyde Avenue
 Mountain View, CA 94042

Grumman Aerospace Corp. (1)
 Bethpage, NY 11714
 Attn: J. Mahon

AVCO Corporation (1)
 Applied Technology Division
 Lowell, MA 01851

North American Aviation (1)
 Columbus Division
 4300 E. Fifth Avenue
 Columbus, OH 43216

Rockwell International Corp. (1)
 12214 Lakewood Blvd.
 Downey, CA 90241
 Attn: M. C. R. Rousseau

McDonnell-Douglas Corp. (1)
 P. O. Box #516
 St. Louis, MO 63166
 Attn: Mr. G. Bilow

General Electric Company (1)
 Valley Forge Space Center
 Philadelphia, PA 19101

Materials Sciences Corp. (1)
 1777 Walton Road
 Blue Bell, PA 19422

U. S. Army Air Mobility R&D Lab. (1)
 Fort Eustis, VA 23064
 Attn: SAVDL-EU-SS (Mr. J. Robinson)

B. F. Goodrich Aerospace & Defense
Products (1)
500 South Main Street
Akron, OH 44318

Lockheed-Georgia Co. (1)
Marietta, GA 30063
Attn: Mr. L. E. Meade

Lockheed Missiles & Space Co. (1)
Synnyvale, CA 94088
Attn: Dr. D. Webster
Dept. 81-35

TRW, Inc. (1)
23555 Euclid Avenue
Cleveland, OH 44117

E. I. DuPont de Nemours & Co. (1)
Textile Fibers Dept.
Wilmington, DE 19898

Bell Aerospace Co. (1)
Buffalo, NY 14240
Attn: Mr. F. M. Anthony

Union Carbide Corp. (1)
Chemicals & Plastics
One River Road
Bound Brook, NJ 08805

General Dynamics (1)
Convair Aerospace Division
P. O. Box 748
Fort Worth, TX 76101
Attn: Tech. Library

General Dynamics (1)
Convair Division
P. O. Box 1128
San Diego, CA 92138
Attn: Mr. W. Scheck
Dept. 572-10

TRW, Inc. (1)
Systems Group
One Space Park, Bldg. 61, Rm. 2171
Redondo Beach, CA 90278

McDonnell-Douglas Corp. (2)
McDonnell Aircraft Co.
P. O. Box 516
St. Louis, MO 63166
Attn: Mr. R. Juergens
Dr. J. Carpenter

Fibers Materials, Inc. (1)
Biddeford Industrial Park
Biddeford, ME 04005
Attn: Mr. J. Herrick

Mr. M. Krenzke (Code 1720)
David W. Taylor Naval Ship R&D Ctr.
Bldg. #19
Bethesda, MD 20084

NASA (1)
Langley Research Center
Hampton, VA 23365
Attn: W. Howell

United Aircraft Corp. (1)
United Aircraft Research Labs.
E. Hartford, CT 06108

United Aircraft Corp. (1)
Pratt & Whitney Aircraft Division
East Hartford, CT 06108

United Aircraft Corp. (1)
Hamilton-Standard Division
Windsor Lock, CT 06096
Attn: Mr. T. Zajac

United Aircraft Corp. (1)
Sikorsky Aircraft Division
Stratford, CT 06602
Mr. J. Ray

Philco-Ford Corp. (1)
Aeronutronic Division
Ford Road
Newport Beach, CA 92663

University of Maryland (1)
College Park, MD 20742
Attn: Dr. W. J. Bailey

University of Wyoming (1)
Mechanical Engineering Dept.
Laramie, WY 82071
Attn: Dr. D. F. Adams

Army Materials & Mechanics
Research Center (2)
Polymers & Chemistry Division
Watertown, MA 02172
Attn: G. L. Hagnauer
R. E. Sacher

Mercules, Inc. (1)
Magna, UT 84044
Attn: R. E. Hoffman

E. I. DuPont Co. (1)
Instrument Products Div.
Concord Plaza
Wilmington, DE 19898
Attn: R. L. Blaine

General Electric R&D Center (1)
Box #8
Schnectady, NY 12301
Attn: Mr. W. Hillig

Stanford Research Institute (1)
333 Ravenwood Avenue
Bldg. #102B
Menlo Park, CA 94025
Attn: Mr. M. Maximovich

University of California (1)
Lawrence Livermore Laboratory
P. O. Box 808
Livermore, CA 94550
Attn: Mr. T. T. Chiao

Northrop Corp. (1)
3901 W. Broadway
Hawthorne, CA 90250
Attn: R. L. Jones
Dept. 3870-62

Pratt & Whitney R&D Center (1)
United Aircraft Corp.
West Palm Beach, FL 33402
Attn: Dr. J. Winfree

Naval Air Propulsion Test Ctr. (1)
Trenton, NJ 08628
Attn: Mr. J. Glatz

Commander (1)
U. S. Naval Weapons Center
China Lake, CA 92555

Naval Ship Engineering Center (1)
Navy Department
Washington, DC 20360
Attn: Code 6101E

Vought Corp. (1)
Systems Division
P. O. Box 6907
Dallas, TX 75222
Attn: G. Bourland

NASA Headquarters (1)
600 Independence Avenue, S.W.
Washington, DC 20546
Attn: Code RV-2
Mr. N. Mayer

The Boeing Company (1)
Aerospace Division
P. O. Box 3707
Seattle, WA 98124

Boeing-Vertol Company (1)
P. O. Box 16858
Philadelphia, PA 19142
Attn: Dept. 1951

STRESS, σ (MPa)

57

10
20
30
40

END

FILMED

1-83

DTIC